
Karl-Franzens University Graz

Bachelor Thesis (BSc)

# Looking for weak jets in proton-proton collisions

Paula Zweynert

Matricular number: 12202706

Supervised by:
Prof. Dr. Axel Maas

13.04.2026

## Abstract

The aim of this thesis is to investigate whether hints of jet-like structures associated with electroweak interactions can be found in proton-proton collisions. For this purpose, events of the process $pp \to \mu^- \mu^+ jjZ$ were simulated using `Herwig`. These data were then analyzed for different systems. The results indicate that no clear signs of weak jets could be found, but information about the kinematics of the different configurations could be obtained.

# Contents

# 1. Introduction

The Standard Model is the foundation of our understanding of the quantum world. However, many processes at small scales are still not fully understood. To further test our current knowledge, experiments such as particle collisions are performed, since high energies correspond to a better resolution of small distance scales. Especially the weak interaction is difficult to investigate experimentally, as its effects are often less dominant than other interactions. Therefore, this thesis aims to investigate jet-like structures associated with electroweak interactions in $pp \to \mu^-\mu^+jjZ$ processes. Such features are often referred to as "weak-jet-like" signatures.

In the following, the necessary theoretical background will be introduced. Afterwards, the methodology and setup will be described in the observables section, and finally, the results will be presented and interpreted in the results section.

# 2. Theory

## 2.1. The Standard Model

The Standard Model (SM), which took shape in its modern form during the 1970s, provides a theoretical framework for describing the elementary particles of the universe and their interactions, including the electromagnetic, weak, and strong forces, with the electromagnetic and weak forces unified in the electroweak theory. However, the remaining fundamental force - gravity - is not accounted for and including it has proven to be a highly difficult task that remains unsolved. Nevertheless, the SM provides an exceptionally accurate description of quantum phenomena, as gravitational effects on such small scales are negligible compared to the other fundamental forces. [1], [2], [3]

In the following tables, all fundamental particles that are currently known, are summarized and categorized into different groups. Since fermions all have antiparticles, an identical table for the corresponding antifermions could be constructed. For the bosons, these are already included in the table. [1]

| | **Fermions** | | |
|---|---|---|---|
| **Leptons** | electron -neutrino $\nu_e$ | muon -neutrino $\nu_\mu$ | tau -neutrino $\nu_\tau$ |
| | electron $e$ | muon $\mu$ | tau $\tau$ |
| **Quarks** | down $d$ | strange $s$ | bottom $b$ |
| | up $u$ | charm $c$ | top $t$ |

Table 1: Fermions [1]

| **Bosons** | |
|---|---|
| $W^{\pm}$-boson | Higgs -boson H |
| $Z$-boson | |
| Photon $\gamma$ | |
| gluon $g$ | |

Table 2: Bosons [1]

These particles interact with each other via four different forces. The first one to be discussed here is the strong force. It is described by the theory of quantum chromodynamics (QCD) and only acts on quarks and gluons. Quarks are treated as the matter fields and the gluons as their massless gauge bosons. Each of these quarks possesses three color charges. But due to confinement only color singlets can be observed. Therefore, quarks can never be observed alone and get pulled together by the strong force to form hadrons, so they appear color neutral to the outside. [2], [4], [5]

The weak force is mediated by the $W^{\pm}$- and $Z$-bosons that act on fermions and each other. Since these bosons are very heavy, the magnitude of the weak force is much smaller than that of the strong force, as well as its reach. It can change particles into one another. A good example of this is the $\beta$-decay $d \to u + W^- \to u + e^- + \bar{\nu_e}$, where a

down-quark transforms into an up-quark by emitting a $W^-$-boson. For 'Charged current' transformations like this, either the $W^-$- or $W^+$- bosons are the acting particles.
'Neutral current' transformations on the other hand, are caused by $Z$-bosons. In these interactions the electric charge does not change (e.g. neutrino-scattering). [3], [5]

Another force that should be mentioned, is the electromagnetic force. It describes the interactions between charged particles through photons and is unified with the weak force to the electroweak theory. But since this theory calls for the gauge bosons to be massless, the Higgs field was introduced. It gives mass to the $W^\pm$- and $Z$-bosons. Thus they can acquire their masses without breaking gauge invariance. [3]

As mentioned before, these three forces are described in the Standard Model, but including gravity posed a challenge since the perturbative quantum gravity is inconsistent. This is due to the fact that the perturbative quantization of general relativity does not work. Therefore, the most popular theories for quantum gravity use a non-perturbative approach. [1], [5], [6]

## 2.2. Particle Collisions

In order to further test and understand the Standard Model, experiments at very small distance scales are required. Since the wavelength $\lambda$ is inversely proportional to the momentum $p$ according to $\lambda = h/p$, very high energies are necessary to achieve an appropriate resolution for such small distances. That is where particle colliders come into play. [7]

A high energy accelerator creates two particle beams with very high momentum and brings them into collision. Typically these beams consist of hadrons e.g. protons at the LHC. [8]

As two of these protons collide, the interactions of their partons (the quarks and gluons that make up the proton) have to be viewed individually. If the momentum transfer between them is very large, hard scattering occurs. In this case three types of collisions are possible: quark-quark, gluon-gluon and quark-gluon. These interactions produce highly energetic partons, also called hard partons. [8], [9]

These high energy partons radiate lower-energy particles e.g. gluons in the so-called parton shower. Such radiation can occur in the initial state of the collision, as well as in

the final state. [9]

Since partons cannot exist on their own due to confinement, they combine with other partons and form color-neutral hadrons, in a process called hadronization. [5], [9]

### 2.2.1. Kinematics

Since the particles that are produced and accelerated in particle colliders reach relativistic velocities, they have to be described using relativistic kinematics. Therefore, this section provides a short introduction to the kinematics of single particles and the relevant relations between two particles before moving on. It should also be mentioned that in the following all units are natural units, if not specified otherwise.

**Kinematics of single particles** When looking at a single moving particle with mass $m$, its energy $E$ and 3-momentum $\mathbf{p}$ can be described with the 4-vector $p = (E, \mathbf{p})$. Its Lorentz-invariant norm can be described by the following formula. [10]

$$p^2 = E^2 - \mid \mathbf{p} \mid^2 = m^2 \tag{1}$$

Because most colliders operate at relativistic velocities, Lorentz-invariant quantities are a convenient way to describe the occurring processes in them. The transverse momentum $p_T$, which is the component of the 3-momentum $\mathbf{p}$ that is orthogonal to the axis of the initial particle beam, is also Lorentz-invariant under boosts along this direction. [9]

Another common way to describe the direction of a particle in collider physics is the pseudorapidity $\eta$ in combination with the azimuthal angle $\phi$. The pseudorapidity is defined by the following formula, with $\theta$ being the polar angle with respect to the beam axis. [9]

$$\eta = -\ln(\tan\tfrac{\theta}{2}) \tag{2}$$

**Kinematics of two particles** Since particle collisions involve more than one particle, it is also important to describe the relations between them. One way to do this is the combined separation variable $\Delta R$, that measures the angular distance between two particles. It is defined by the following formula, with the relative azimuthal angle being

$\Delta\phi = \phi_1 - \phi_2$ and the relative pseudorapidity $\Delta\eta = \eta_1 - \eta_2$. [9], [11]

$$\Delta R = \sqrt{(\Delta\eta)^2 + (\Delta\phi)^2} \tag{3}$$

Furthermore the total center-of-mass energy $\sqrt{S}$ of two particles can be calculated from their 4-momenta $p_1$ and $p_2$. Conveniently this quantity is also Lorentz-invariant. [10], [12]

$$\sqrt{S} = \sqrt{(p_1 + p_2)^2} \tag{4}$$

The most important ingredients for jet definition and later analysis have now been established. Therefore, the concept of jets can be introduced.

## 2.3. Jets

When a parton shower occurs in a high-energy collider, the detector will measure a collimated spray of hadronized particles. Since they all originate from the same high-energy parton, they can be reconstructed as a single object, called a jet. It can be treated as such an object and has well-defined kinematic properties, including the 4-momentum, which is just the sum of all 4-momenta of the particles it is formed of. [8]

### 2.3.1. Jet Algorithms

A jet algorithm is a procedure to reconstruct a jet from the particles it is composed of. Two of the most commonly used ones are cone and clustering algorithms. Since in this thesis only a specific clustering-algorithm was required, it will be the only one discussed in detail. [13]

To reconstruct a jet with the Durham clustering algorithm, first the distances between all possible particle pairs $y_{ij}$ are calculated using the following equation. $E_i$ and $E_j$ are the energy of the respective particle and $cos(\theta_{ij})$ is the spatial angle between them. [14]

$$y_{ij} = \frac{2min(E_i^2, E_j^2)}{(E_i + E_j)^2}(1 - cos(\theta_{i,j})) \tag{5}$$

When the distances for all particle pairs are calculated, the smallest one is selected and compared to a cut-off parameter $y_{cut}$. If it is smaller than $y_{cut}$, the two particles get clustered into a new pseudoparticle. Then the distances $y_{ij}$ have to be calculated again,

but this time with the new pseudoparticle. This has to be repeated until the break condition $y_{min} > y_{cut}$ is met. In this case all remaining particles and pseudoparticles are considered jets. [14]

### 2.3.2. Electroweak Jets

The word jet is a very broadly defined term, but most of the time "jet" will refer to a QCD jet. It is a jet that is created by the parton shower initiated by a parton. That means that the strong force is mainly responsible for QCD jets. But in addition to QCD jets, there exist other types of jets.
One of these jets is the electroweak jet. Since hadron-colliders operate at very high energies, the partons carry enough momentum to be able to radiate a $W^{\pm}/Z$-boson, which is a gauge boson of the weak force. The particle spray created from such a decaying $W^{\pm}/Z$-boson is then called a weak jet.
Since it has turned out to be rather difficult to distinguish a QCD jet from a weak jet, it has not been easy to identify them in experiments. But especially at high energies electroweak corrections become more important, which is why they cannot be neglected anymore. Because of this, the scientific interest in weak jets has risen over the past years in order to find better ways to include electroweak effects in jet reconstruction and simulations. [15]

## 2.4. Herwig

In order to make predictions for the processes in a high-energy collider, Monte Carlo generators are used to simulate these events. One of them is "`Herwig`". It can simulate a number of hard scattering processes, the resulting parton showers, the underlying event, as well as the hadronization. [16] [17]

To decide which partons collide with each other in a hard scattering process, Herwig uses built-in parton distribution functions (PDFs) that are assigned to the beam particles. From these PDFs, Herwig samples the momentum fractions of the incoming partons. For the $2 \to 2$-collisions, Herwig includes a library of matrix elements for QCD, electroweak and supersymmetric subprocesses. The resulting kinematic properties of the two particles define the initial conditions for the parton showers. They are simulated with an angular-ordered shower model. [16] [17] [18]

To generate an event in Herwig, a number of initial parameters, as well as a process code,

are required. These parameters include the particle beam names, their momenta and the number of required events.
The output of such an event can then be examined by performing an analysis, which has to be written by the user. [16], [17]

# 3. Observables

To investigate high-energy proton-proton collisions and the weak jets occurring in them, the first step was to perform a Monte Carlo simulation. For this purpose, the `Herwig` 7.3.0 environment was set up and the input file `sm.in` was read using `Herwig read sm.in`, which contains all the setup parameters for the desired simulated collisions. In this case the desired process was $pp \rightarrow \mu^-\mu^+jjZ$ at a center-of-mass energy of $\sqrt{S} = 13$ TeV. The matrix elements were generated with `MadGraph` within the framework of `Matchbox` and the PDF set `MMHT2014` was used. Furthermore, parton showers and cascades, as well as the hadronization and particle decays were disabled and the five-flavor scheme was employed including the quark flavors u, d, s, c and b. Using this setup, 50,000 events were generated with `Herwig run sm.run -N 50000` and saved in an `.hepmc` file. [19], [20], [21], [22], [23], [24], [25], [26], [27]

These events were then analyzed using different `C++` analysis routines within the `Rivet 3.1.8` framework, that are provided in Appendix 1. The resulting observables were calculated in the laboratory frame and the computed distributions were normalized. Additionally, all events were treated as unweighted. The visual representation of the data was produced using `MATLAB`. Further details on the specific distributions will be discussed in the following sections.

## 3.1. Muon - Antimuon

The first objective was to analyze the energetic and spatial relationship between muon-antimuon pairs. For this purpose, the pseudorapidity $\eta$ was evaluated for the individual particles of the leading $\mu^-\mu^+$ pair of each event. Then the pseudorapidity difference $\Delta\eta = \eta_1 - \eta_2$ was computed and plotted to measure the longitudinal separation along the beam axis between the particles. A similar procedure was applied to measure the angular distribution $\Delta\phi$ between said particle pairs in order to analyze their transverse correlation. Since the azimuthal angle $\phi$ is periodic with $2\pi$, the periodicity was taken into account when calculating $\Delta\phi$.
Then $\Delta R$ was calculated with $\Delta\phi$ and $\Delta\eta$ according to formula 3 for each particle pair to measure the angular separation in $\eta - \phi$ space between the particles. The resulting $\Delta R$ distribution for all particle pairs was then displayed in a histogram.
In order to further investigate the kinematic separation of the particles, the Durham distribution $y_{ij}$ was also calculated. First the particle energies $E_i, E_j$ were extracted and then the angular separation $\theta_{ij}$ between them. Then these observables were used in

equation 5 to compute $y_{ij}$. The resulting Durham distribution for all events was then plotted after applying the natural logarithm to the x-axis, since it spans several orders of magnitude.

The corresponding analysis routine for these calculations can be found in the Appendix 1.

## 3.2. Muon - Z

Next the relation between a muon and Z boson was investigated. To do so, the pseudorapidity difference $\Delta\eta$ and the angular separation $\Delta\phi$ between these particles were plotted and used to calculate $\Delta R$ as described in the previous section. Then the square root of the center-of-mass energy $\sqrt{S}$ was computed by inserting the extracted 4-momenta $p_{\mu^-}, p_Z$ of the muon and Z boson in equation 4. Together $\Delta R$ and $\sqrt{S}$ were then plotted in a heatmap using a 10 x 10 binning and a range of $\Delta R \in [0, 6]$ and $\sqrt{S} \in [0, 500]$ GeV. The aim here was to see whether the number of jets, defined as the number of objects satisfying $\Delta R < R_j$, would rise with $\sqrt{S}$, since this could indicate weak-jet-like behavior. The corresponding Durham distribution $y_{ij}$ for these particles was then plotted logarithmically in a histogram following the same procedure as in Section 3.1.

Details of the implementation are provided in Appendix 2.

## 3.3. Higher-energy muon - Z

A similar investigation was performed for the relation between the higher-energy muon of a muon-antimuon pair and a Z boson. This particle was identified in each event and then compared to the Z boson as described in the previous section. Apart from the particle selection, all other calculations and plots were carried out in the same way as described in section 3.2. The objective of this section also remained the same as before, with the difference that the higher-energy muon may carry a larger fraction of the event kinematics and could therefore exhibit a stronger correlation with the Z boson.
The code for the analysis in this chapter can be found in the Appendix 3.

## 3.4. Higher-energy muon - Z cone jet

Attention was then directed towards the construction of cone-based jets. For this purpose a cone with the radius $R0$ was constructed around the higher-energy muon. If the Z boson was within this cone, the event was included in the analysis, otherwise, it was

discarded. The Z boson within this cone was then compared to the higher-energy muon, following the same procedure as in Section 3.2. To evaluate the impact of the cone radius $R0$, the heatmap was plotted for $R0 = 0.4$ and $R0 = 0.8$. The heatmap for $R0 = 0.8$ was then plotted again with adjusted limits and a 50 x 100 binning. The limits of this plot were $\Delta R \in [0, 0.8]$ and $\sqrt{S} \in [0, 350]$, but the region $\sqrt{S} \in [0, 100]$ was not shown, since this part of the graph was entirely empty. The purpose of these plots was to search for weak-jet-like behavior in the constructed jet.
Additionally, the $\Delta\eta$ and $\Delta\phi$ distributions were plotted twice. One with coarse binning and one with finer binning to resolve the structure of the distributions. The Durham distribution was also plotted again following the same steps as in the previous sections, except that this time two graphs were plotted for $R0 = 0.4$ and $R0 = 0.8$.

See Appendix 4 for the corresponding code.

### 3.5. Higher-energy muon - jj

Furthermore, the analysis was extended to QCD jets. For this purpose a cone around the higher-energy muon was defined again. This time all particles of the final state within this cone, except for neutrinos and the higher-energy muon, were defined as a jet. The cone radius $R0$ was then varied and two heatmaps for $R0 = 0.4$ and $R0 = 0.8$ were plotted, following the same procedure as described in the previous section. Then a zoom of $R0 = 0.8$ was computed, with $\Delta R \in [0, 2]$ and $\sqrt{S} \in [0, 400]$ and a higher binning of 50 x 100 to see more structure in the plot. Since the heatmap was empty for $\Delta R > 0.8$ due to the jet definition, only $\Delta R \in [0, 0.8]$ was displayed. The range $\sqrt{S} \in [300, 500]$ was not displayed, as it also contained no events. The purpose here was to look for weak-jet-like behavior.
The $\Delta\eta$ and $\Delta\phi$ distributions, as well as the Durham distribution, were then plotted in the same way as described in the previous section.

The analysis routine used here is documented in Appendix 5.

# 4. Results

In the following chapter, the computed graphs will be discussed and interpreted.

It should be noted that only Monte-Carlo uncertainties were considered, with the biggest source of uncertainty being the finite number of events. This leads to Poisson statistics, and the error can be calculated as $\sigma = \sqrt{N}$, with N being the number of events per bin. In the histograms, the resulting error was depicted in the graphs, using error bars, whereas for the heatmaps a short error discussion will be provided in the text.

## 4.1. Muon - Antimuon

The first observable to be discussed is the pseudorapidity difference $\Delta\eta$. As can be seen in the graph, the relative uncertainties around the peak were small enough to allow an analysis of the trend.

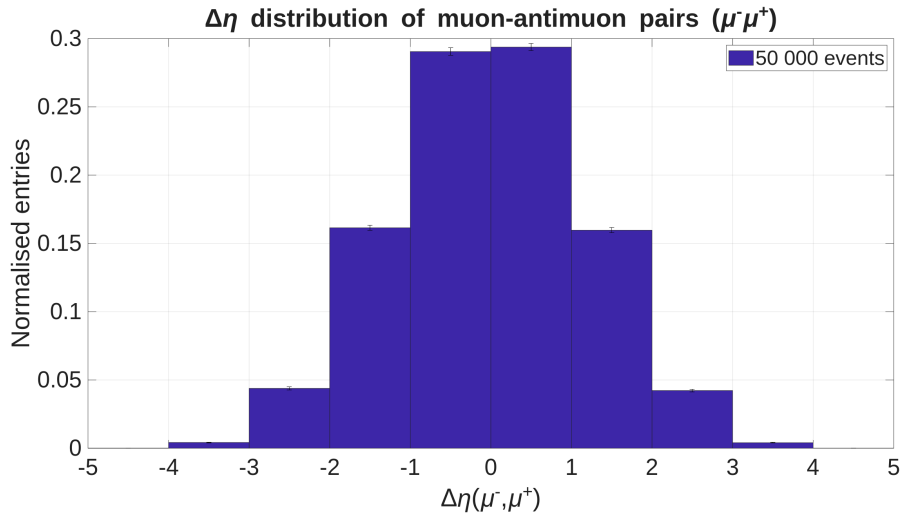


Figure 1: Distribution of the pseudorapidity difference $\Delta\eta$ for leading muon-antimuon pairs in a sample of 50 000 events.

There are two interesting pieces of information that can be obtained from this graph: the rough location of the peak, and the shape of the distribution. In this case, the peak was symmetric around zero with a Gaussian-like shape.

The peak around zero can be interpreted in a way that the muon-antimuon pair is often emitted with similar pseudorapidities, since $\Delta\eta = \eta_{\mu^-} - \eta_{\mu^+}$. In other words, they tend to be emitted with a similar polar angle relative to the beam axis. As this observable is also invariant under longitudinal boosts, the longitudinal boost due to relativistic velocities of the particle pair did not have to be considered.
Since the distribution lies within the interval [-4,4], the muon-antimuon pairs did not always have a similar pseudorapidity, but could also have significantly different polar angles, due to longitudinal boosts of the system and underlying event kinematics. The peak just indicates that most particles followed this trend.

The angular distribution difference $\Delta\phi$ can give further information about the kinematic relationship of the particle pairs.

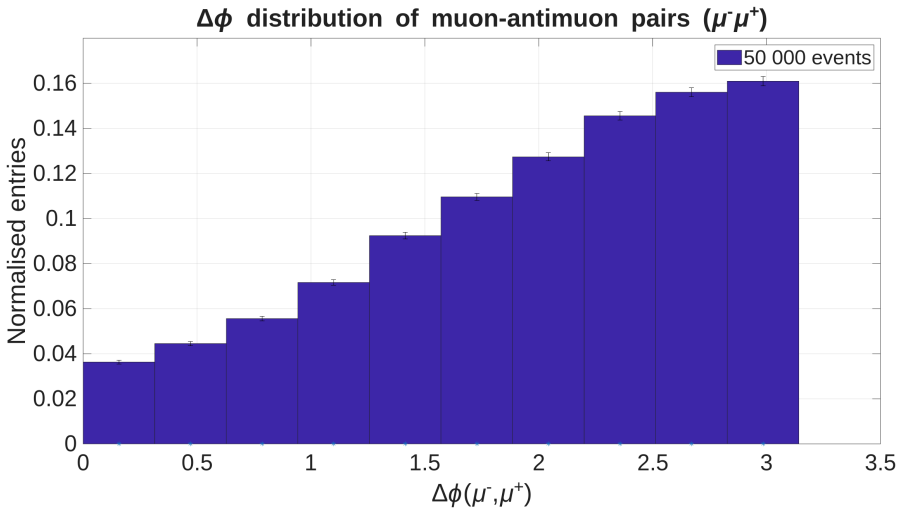


Figure 2: Distribution of the azimuthal angle difference $\Delta\phi$ for leading muon-antimuon pairs in a sample of 50 000 events.

This graph shows a peak at approximately $\pi$ and a very flat curve. The peak at $\pi$ indicates a back-to-back behavior of the muons in the transverse plane, since the initial transverse momentum was zero and therefore the other muon has to fly in the opposite direction to conserve the transverse momentum. The range of $[0,\pi]$ on the other hand indicates that the muon-antimuon system does not always have a transverse momentum of zero. This is expected, since other particles - e.g. particles within the jets - can absorb some of the momentum.

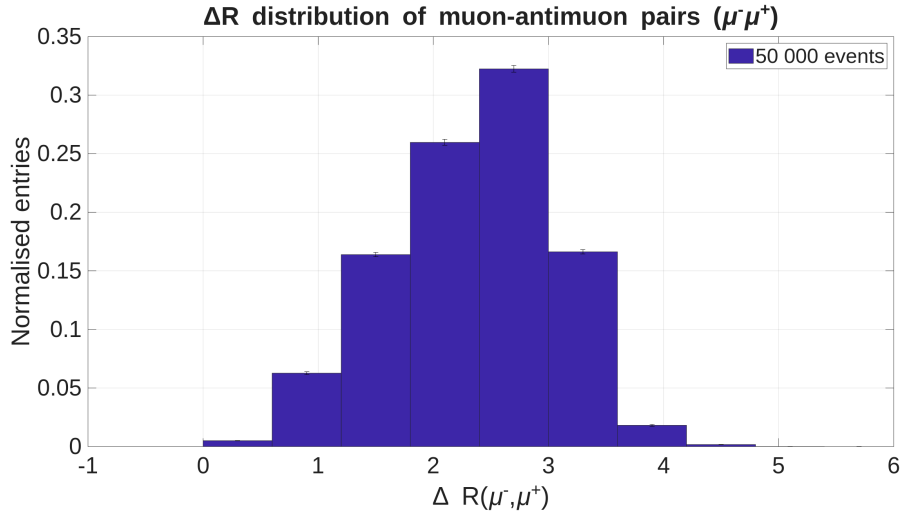


Figure 3: Distribution of $\Delta R$ for leading muon-antimuon pairs in a sample of 50 000 events.

Since the $\Delta R$ distribution combines the longitudinal $\Delta\eta$ and transverse separation $\Delta\phi$, it is a measure of the geometrical separation of two objects. The fact that the peak is not exactly at $\pi$ but a little shifted to smaller values is consistent with the previous assumption that many, but not all muon-antimuon pairs show a back-to-back behavior. Since the $\Delta\phi$ distribution cannot be greater than $\pi$, the values in the $\Delta R$ distribution higher than $\pi$ can be attributed to the events with non-zero $\mid \Delta\eta \mid$.
Therefore, it can be said that the $\Delta R$ distribution is consistent with the previous assumptions that the muon-antimuon pairs are generally emitted with a similar polar angle and back-to-back in the transverse plane.

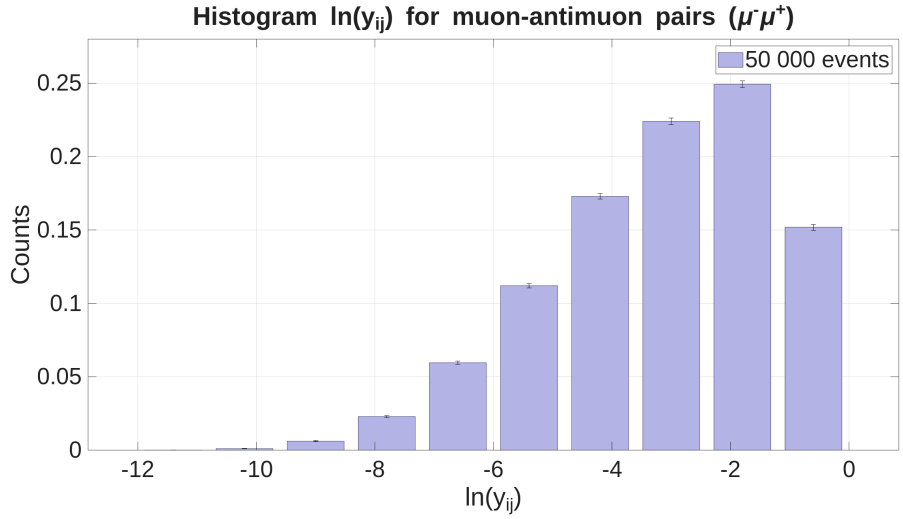


Figure 4: Logarithmic distribution of the Durham variable for leading muon-antimuon pairs in a sample of 50 000 events.

The Durham distribution $y_{ij}$ measures the symmetry of a muon-antimuon pair by evaluating the energy ratio between the particles and their geometrical separation. Since the previously calculated distributions were never concentrated in just one point, it has to be kept in mind that these values are just the most likely outcome and not an absolute measure for the following interpretation. If it is assumed that the $\Delta\phi$ distribution lies at $\pi$, since its peak was located there and the $\Delta\eta$ distribution at 0, the geometrical separation $\theta_{ij}$ can be approximated by $\theta_{ij} \approx \Delta\phi \approx \pi$. When this value is inserted in the angular term of equation 5, the term becomes $(1 - cos\theta_{ij}) \to 2$. Therefore, the outcome would largely depend on the energy term. Since the peak lies at $\ln(y_{ij}) \approx -1.8$, the value of the peak is $e^{-1.8} \approx 0.165$. That is a moderately small value, but assuming that the geometrical term really is 2, this could indicate that the particle pairs are not perfectly symmetric.
However, it should be emphasized that this conclusion relies on several simplifying approximations and should therefore be treated with caution.

## 4.2. Muon - Z

In the following, the results of the relation between muons and Z bosons are discussed. Since representing errors in a heatmap is challenging, the error discussion is provided in the text. In the following heatmap, the well-populated bins have a relative error of approximately 2%, while low-statistics regions show relative uncertainties of up to $\approx 40\%$.

The relative error was calculated by dividing the statistical error by the number of events in each bin. Some bins are empty and therefore do not have a defined relative error. For this reason, only the regions with sufficient statistics are discussed below, since only these regions exhibit sufficiently small uncertainties to allow a meaningful interpretation of the trend.

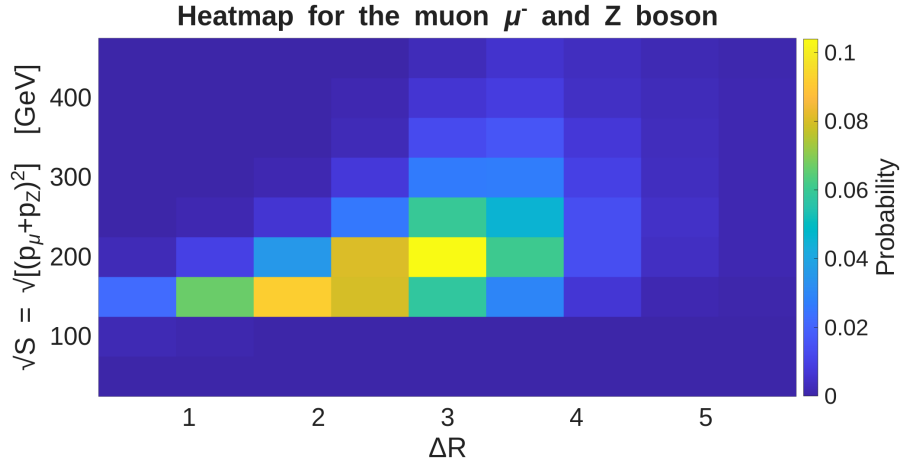


Figure 5: Globally normalized heatmap of $\Delta R$ as a function of $\sqrt{S}$ for the $\mu^-$-Z system in a sample of 50 000 events.

This heatmap shows the relation between $\Delta R$ and $\sqrt{S}$ for a muon $\mu^-$ and a Z boson. Since the heatmap was globally normalized, the bin colors only show the probability of an event occurring. The brighter bins indicate a higher probability. In this heatmap, an upward curve can be observed. This indicates a positive correlation between $\Delta R$ and $\sqrt{S}$. The bins from (0-100) GeV are likely empty, as a Z boson on its own already has a mass of $\sqrt{S} \approx 90$ GeV. Therefore, values below this are not expected.
When looking for weak jets in this heatmap, one would expect to see a decreasing $\Delta R$ with increasing $\sqrt{S}$. This is because a weak jet could in this case be caused by electroweak radiation associated with the muon. Since these two particles would become more collimated with increasing energy, higher-energy would lead to smaller $\Delta R$. Therefore, a peak in the region of small $\Delta R$ and large $\sqrt{S}$ would be a sign for weak-jet-like behavior. A feature like this is not clearly observed in the graph. That does not necessarily mean that it did not occur, but it is possible that limited statistics obscure potential effects. It can therefore only be concluded that this graph does not show clear signs for weak jets. Since this is not clearly observed, the Z production cannot be conclusively associated with the muon.

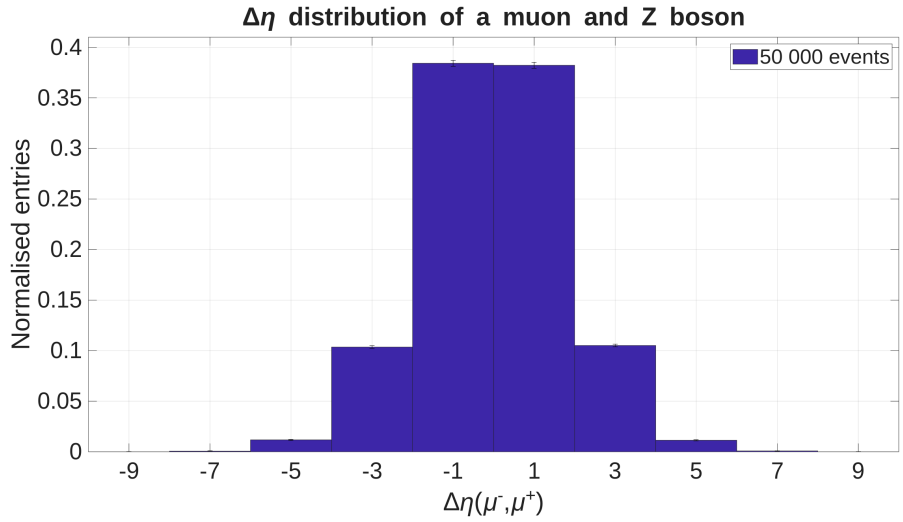


Figure 6: Distribution of the pseudorapidity difference $\Delta\eta$ for the $\mu^-$-Z system in a sample of 50 000 events.

Regarding the $\Delta\eta$ distribution, a similar behavior to that in the previous section can be observed. It has a symmetric Gaussian-like shape that peaks at $\Delta\eta \approx 0$. As before, this indicates that the two particles - in this case the muon and the Z boson - are likely to be emitted with similar pseudorapidity values $\eta$.

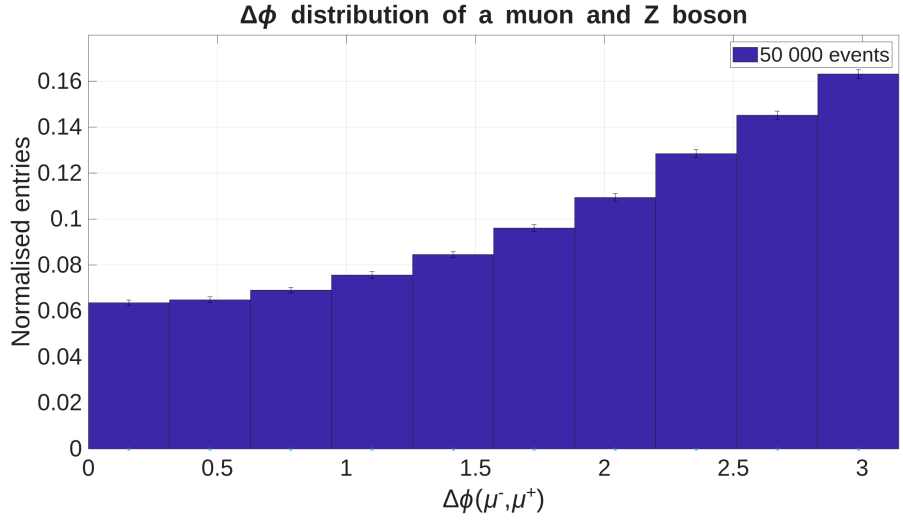


Figure 7: Distribution of the azimuthal angle difference $\Delta\phi$ for the $\mu^- - Z$ system in a sample of 50 000 events.

The $\Delta\phi$ distribution also shows a similar trend to that observed in the previous section. It continuously rises in the interval $[0,\pi]$, which it cannot exceed by definition and peaks in the last bin around $\Delta\phi \approx 2.9$. Since the peak is even sharper than in Figure 2, this suggests even more strongly that the muon and the Z boson have a high probability of exhibiting back-to-back behavior in the transverse plane.

Considering the previous two distributions, this suggests that the muon and the Z boson are produced with similar pseudorapidities while being back-to-back in the transverse plane. This also aligns well with the fact that in the heatmap 5 a peak around $\Delta R \approx \pi$ was observed.

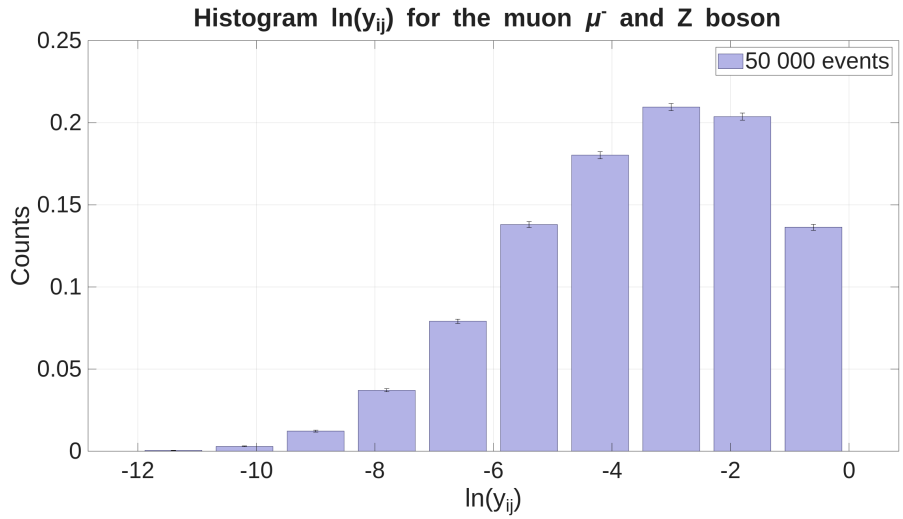


Figure 8: Logarithmic distribution of the Durham variable for the $\mu^- - Z$ system in a sample of 50 000 events.

Taking the previous assumptions into account, this indicates that the angular separation $\theta_{ij}$ is rather big. As derived in chapter 4.1, this means that the formula would have to depend on the energy term to obtain the observed peak value of $\ln y_{ij} \approx -3$, suggesting that there is a substantial asymmetry between the energies of the two particles.

## 4.3. Higher-energy muon - Z

The relative error for this heatmap is very similar to the previous one. In high-statistics regions, the error ranges between $1\% - 3\%$, while the moderately populated regions display a relative error of about 5%. In regions with very low statistics the error increases

significantly and reaches values up to 50%. Therefore, only bins with sufficiently small uncertainties are considered in the interpretation.

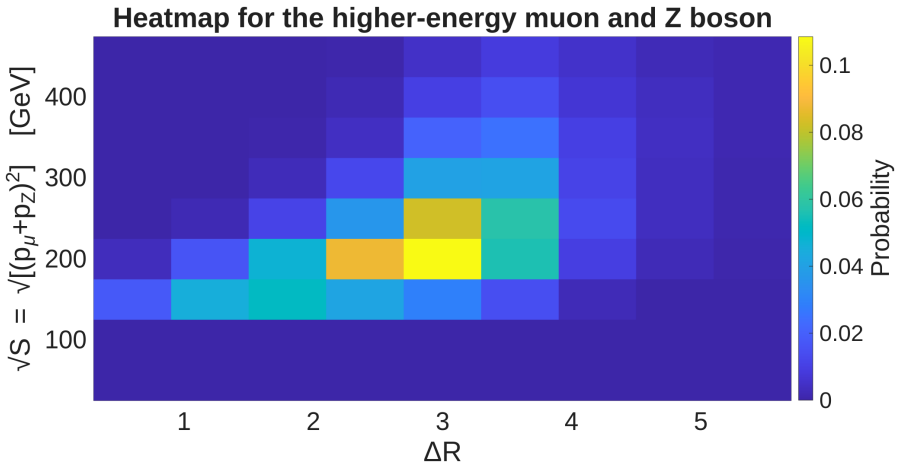


Figure 9: Globally normalized heatmap of $\Delta R$ as a function of $\sqrt{S}$ for the higher-energy muon and the Z boson in a sample of 50 000 events.

Compared to the previous heatmap 5, the peak here is considerably sharper and can be found at approximately $\Delta R \approx 3$. This increase in sharpness could indicate that the Z boson has a higher chance of being back-to-back with the higher-energy muon, which is likely due to the fact that the transverse momentum in a collision has to be conserved. Since the Z boson and higher-energy muon carry a large portion of the momentum, they are also more likely to exhibit back-to-back behavior. The lower-energy muon carries less momentum and can therefore be influenced more easily by the jets. This could explain why the peak that indicates back-to-back behavior sharpens when only the higher-energy muons are considered.
A clear sign of weak jets cannot be found in the heatmap, because the bins for small $\Delta R$ and large $\sqrt{S}$ are empty. However, as before, an upward trend can be observed, indicating a correlation between $\Delta R$ and $\sqrt{S}$ for the higher-energy muon and the Z boson.

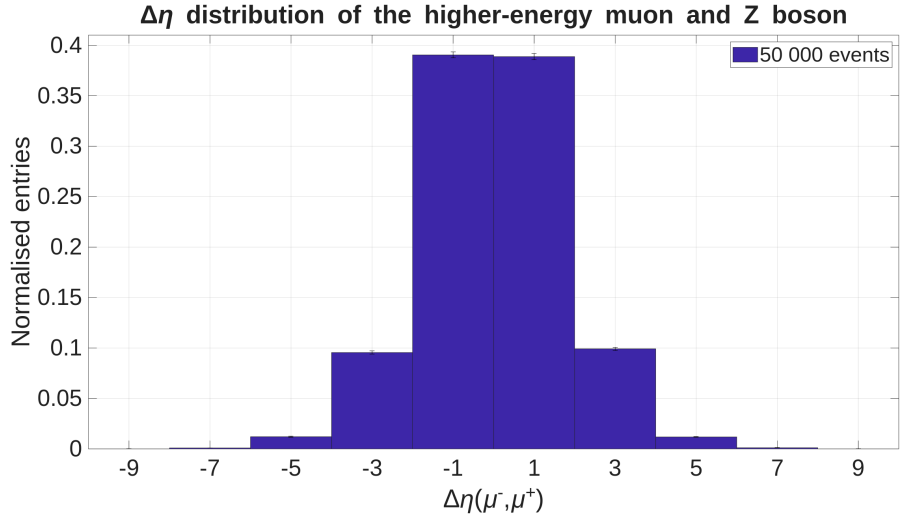


Figure 10: Distribution of the pseudorapidity difference $\Delta\eta$ for the higher-energy muon and the Z boson in a sample of 50 000 events.

The peak of the pseudorapidity difference $\Delta\eta$ is also slightly more distinct compared to the $\Delta\eta$ distribution of the muon-Z system shown in Figure 1, which is consistent with the previous assumptions. Otherwise, no major changes of the distribution are observed and therefore the implication that the higher-energy muon and the Z boson are likely to have similar pseudorapidity values still stands.

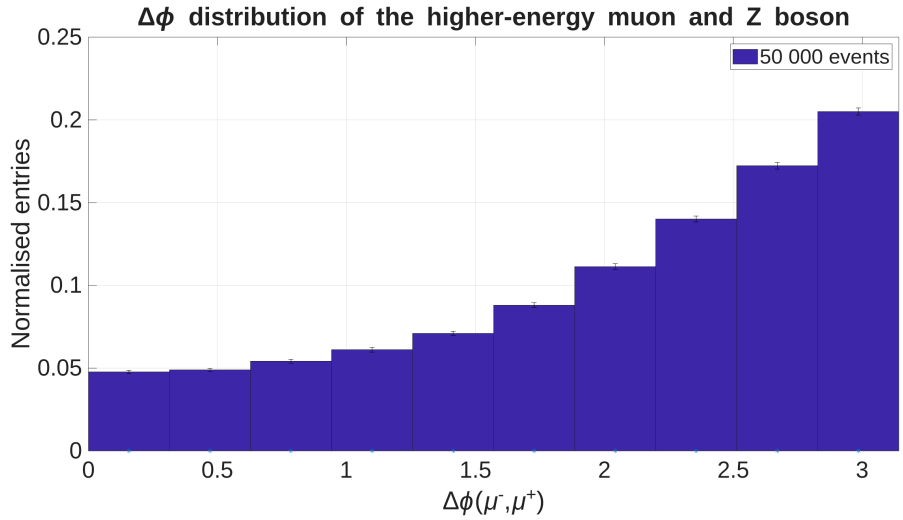


Figure 11: Distribution of the azimuthal angle difference $\Delta\phi$ for the higher-energy muon and the Z boson in a sample of 50 000 events.

The $\Delta\phi$ distribution also shows a very similar trend to the one observed in the previous section, with an upward curve that ends with a peak at $\Delta\phi \approx \pi$. But in this graph, the curve starts with lower values for small $\Delta\phi$ and the peak is more pronounced. This supports the previously made assumption that the higher-energy muon is more strongly back-to-back correlated with the Z boson than the lower-energy muon.

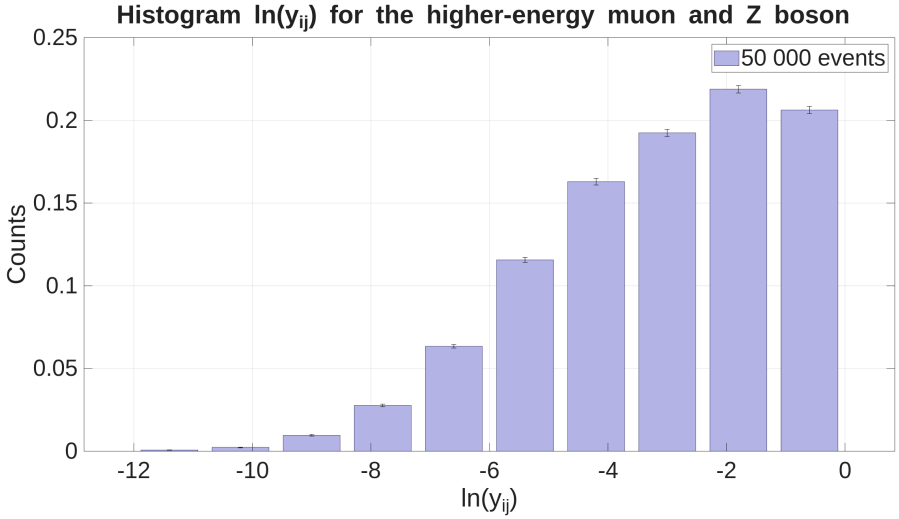


Figure 12: Logarithmic distribution of the Durham variable for the higher-energy muon and the Z boson in a sample of 50 000 events.

As can be seen in Figure 12, the logarithmic Durham distribution has a peak at $\ln y_{ij} \approx -1.8$. That is a larger value than in the muon-Z distribution. Taking the previous assumptions into account, this could be due to the fact that the angular separation term increased, because the higher-energy muon and the Z boson are more strongly back-to-back correlated. Another contribution comes from the energy term. Since the higher-energy muon is more likely to be closer in energy to the Z boson than the lower-energy muon, the energy term in equation 5 would also increase.

Therefore, the graphs suggest that the higher-energy muon is more strongly back-to-back correlated with the Z boson than the lower-energy one. Since this behavior does not provide evidence for weak jets and no significant increase in the number of jets within a radius $R0$ with increasing $\sqrt{S}$ could be observed, it can be concluded that no definite sign of weak jets was found.

## 4.4. Higher-energy muon - Z cone jet

For this chapter, two heatmaps were plotted to study the effect of different cone radii $R0$. Since they are both mainly empty, with few bright bins, there is no useful uncertainty discussion to be conducted for these empty areas, which is why only the filled bins will be discussed. The heatmap with a cone radius $R0 = 0.4$ displays two bright bins with relative uncertainties of $5\% - 13\%$. A few additional bins also contain entries, but they are barely visible and have very large uncertainties of about $60\% - 100\%$ and are therefore not considered further. The sparsely populated bins in the heatmap for $R0 = 0.8$ show a similar behavior. Only the four highly populated bins with relative uncertainties of $4\% - 15\%$ have sufficiently small uncertainties to allow interpretation.

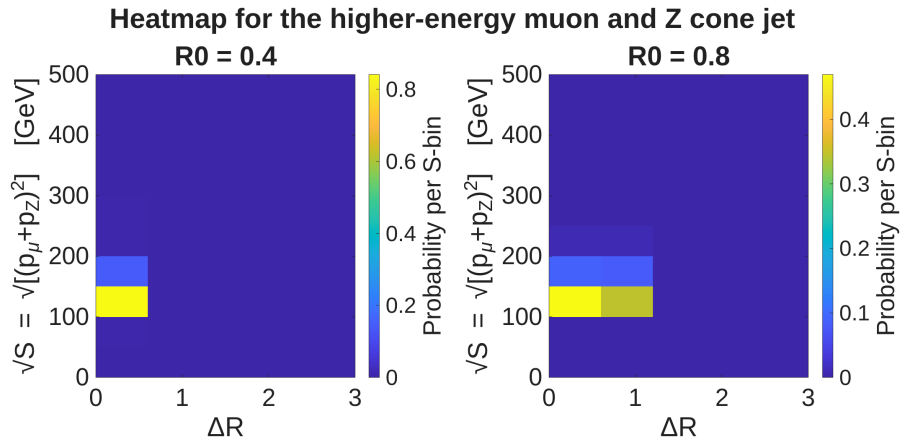


Figure 13: Globally normalized heatmap of $\Delta R$ as a function of $\sqrt{S}$ for the higher-energy muon and the Z cone jet in a sample of 50 000 events. The left (right) panel corresponds to a cone radius of $R0 = 0.4$ ($R0 = 0.8$).

Both heatmaps display sharp peaks at small $\Delta R$, which indicates small angular separation between the Z boson and the higher-energy muon. That is consistent with expectations since the code 4 purposefully excluded events with large angular separation. Therefore, a larger number of populated bins for the larger cone radius is expected, since a larger cone selects more events.

To observe the internal structure of these peaks, the heatmap with cone radius $R0 = 0.8$ was plotted again with a finer binning and smaller axis limits. This significantly increased the relative uncertainty of each bin. The highly populated bins display a relative uncertainty of approximately 28% while the less populated ones have uncertainties of

$45\% - 60\%$. The empty bins will again be disregarded.

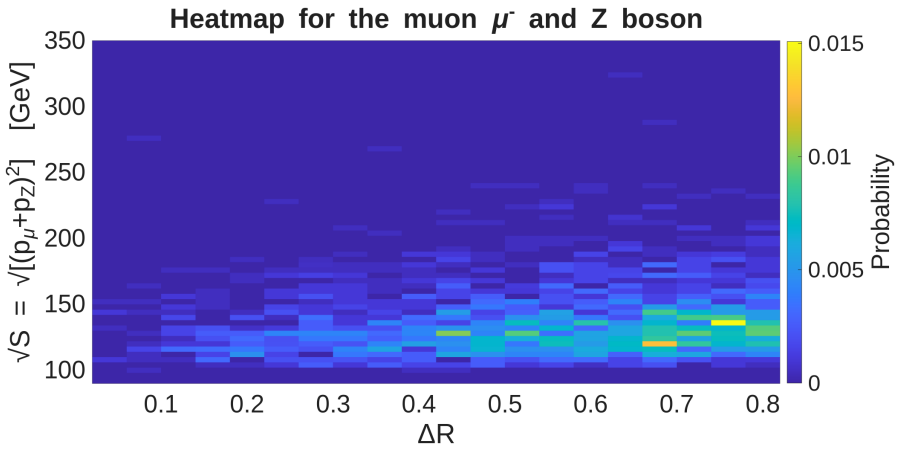


Figure 14: Globally normalized heatmap of $\Delta R$ as a function of $\sqrt{S}$ for the higher-energy muon and the Z cone jet in a sample of 50 000 events, shown for a cone radius of $R0 = 0.8$ with finer binning and a zoomed-in range.

Since the cone was only defined within $R0 = 0.8$, the graph was cut off at this value. What can be seen here is an extended peak along the x-axis that increases for larger $\Delta R$. Its y-value lies at $\sqrt{S} \approx 125$ GeV. This value is close to the mass of the Higgs boson [28]. However, since not the entire system - in this case $\mu^-\mu^+Z$ - was considered, no definite identification of the Higgs boson can be made.
When looking for weak jets, one would expect more events at higher energies $\sqrt{S}$, which could not be observed in this graph nor in the previous heatmaps 13. Therefore, no clear indication of weak jets was found.

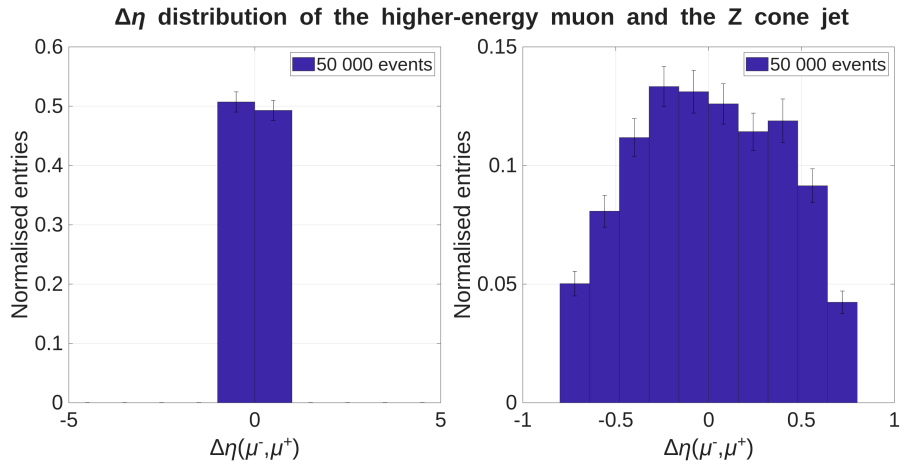


Figure 15: Distribution of the pseudorapidity difference $\Delta\eta$ for the higher-energy muon and the Z cone jet in a sample of 50 000 events. The left (right) panel shows the distribution with coarser binning (a zoomed-in view) for a cone radius of $R0 = 0.8$.

The pseudorapidity difference distribution shows a peak around zero that significantly increased in sharpness compared to the previous section. This behavior was expected, as the constructed cone selects particles that have a $\Delta R < R0$. Using this relation, with $\Delta R = \sqrt{(\Delta\eta) + (\Delta\phi)}$ the maximal pseudorapidity difference that can be achieved is $\mid \Delta\eta \mid \leq R0$. To further investigate the barely visible structure of this distribution, another plot with a finer binning was generated. Taking the uncertainties into account, it is approximately symmetric around zero and shows nothing unexpected. Therefore, it will not be discussed further.

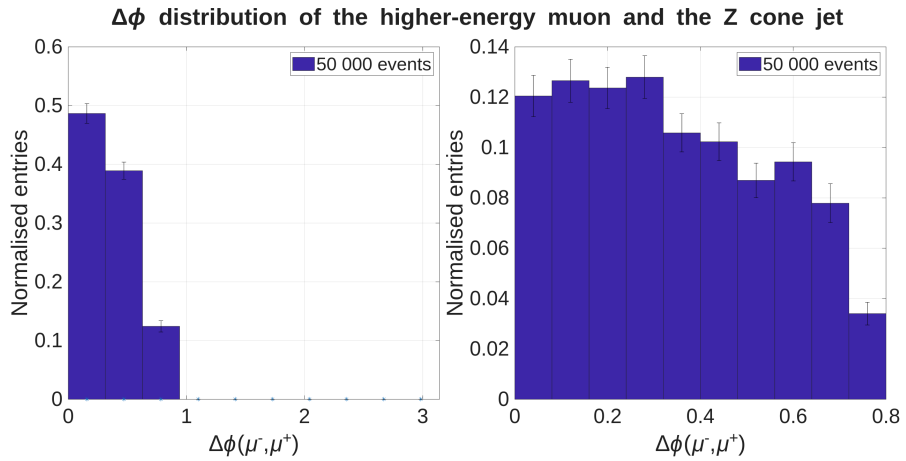


Figure 16: Distribution of the azimuthal angle difference $\Delta\phi$ for the higher-energy muon and the Z cone jet in a sample of 50 000 events. The left (right) panel shows a distribution with coarser binning (a zoomed-in view) for a cone radius of $R0 = 0.8$.

In Figure 16 a peak of the angular separation distribution at $\Delta\phi \approx 0$ can be observed. That indicates a collimated system. This suggests a correlation between the higher-energy muon and the Z boson, considering that $\Delta\eta$ also peaked close to zero. The distribution with a finer binning also reveals no structure that is not consistent with the broader one. Hence, no further discussion will be given.

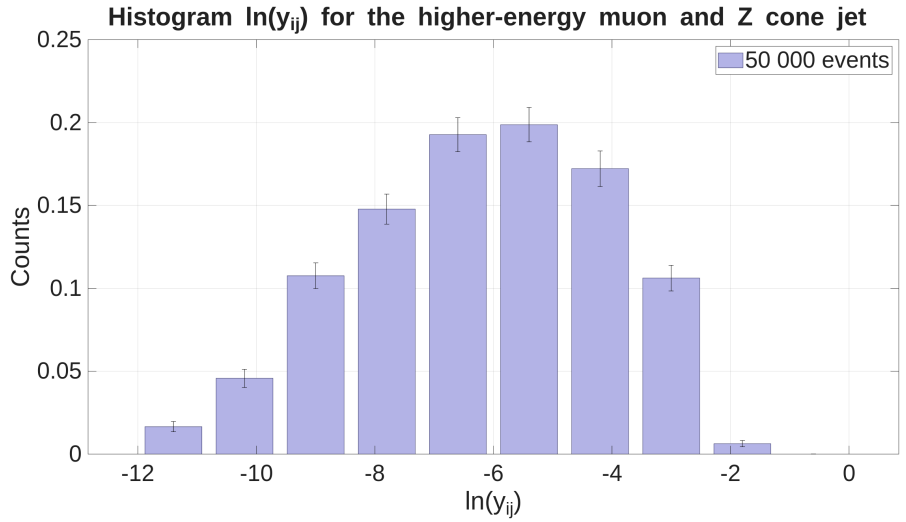


Figure 17: Logarithmic distribution of the Durham variable for the higher-energy muon and the Z cone jet in a sample of 50 000 events for the cone radius $R0 = 0.8$.

Next, the Durham distribution was plotted. It shows a peak at $\ln(y_{ij}) \approx -5.5$, which hints at a collinear relationship between the higher-energy muon and the Z boson and therefore is consistent with the previous graphs of this section. However, an energy asymmetry cannot be ruled out as the cause of the peak. Nevertheless, together with the $\Delta\eta$ and $\Delta\phi$ distributions, it is suggested that collinearity did occur to some degree.

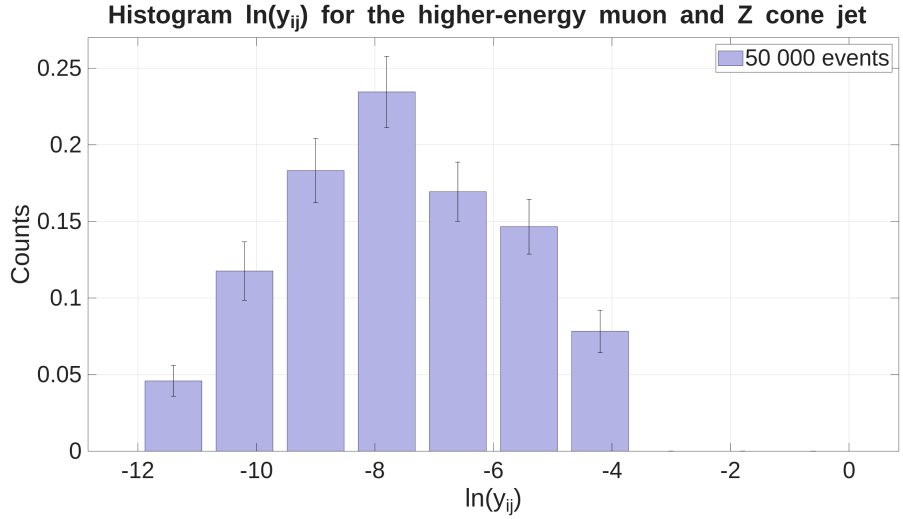


Figure 18: Logarithmic distribution of the Durham variable for the higher-energy muon and the Z cone jet in a sample of 50 000 events for the cone radius $R0 = 0.4$.

Compared to the previous distribution, the peak of the Durham distribution for $R0 = 0.4$ is even more shifted toward smaller values at $\ln(y_{ij}) \approx -7.9$. A possible explanation for this is that for a smaller $R0$ smaller angular separations are selected. Since the Durham distribution is proportional to $(1 - \cos\theta)$, the peak is expected to shift to smaller values. The energy term could also play a role in this.

Together with the previous graphs this shows a consistent picture, in which the selection of the cone ensures that only particles with small angular separation are selected. The results also show a collimated configuration of the particles, with increasing collinearity for smaller cone radii. An energy asymmetry could also play a role in this. Weak-jet-like behavior was not observed.

## 4.5. Higher-energy muon - jj

Similar to before, the heatmaps of the constructed jet with respect to the higher-energy muon were plotted for different cone radii $R0$. Their relative uncertainty also remained moderate in the highly filled bins of the lower-left corner and increased significantly in the other regions.

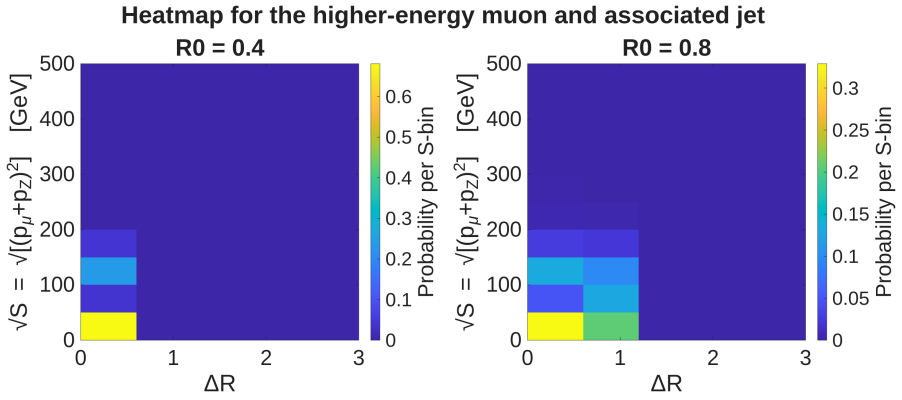


Figure 19: Globally normalized heatmap of $\Delta R$ as a function of $\sqrt{S}$ for the higher-energy muon and the associated jet in a sample of 50 000 events. The left (right) panel corresponds to a cone radius of $R0 = 0.4$ ($R0 = 0.8$).

Compared to the heatmaps 13 of the previous section these heatmaps are better populated, which is consistent with expectations, since in this analysis all particles within the constructed cone were considered, whereas before this was only done for the Z boson. Therefore, more particles could contribute to the energy and subsequently populate more bins. Nevertheless, the binning was not sufficient to observe any significant structure, which is why the heatmap for $R0 = 0.8$ was plotted again with finer binning and new axis limits.

The statistical precision of this figure is relatively low, since a fine binning was chosen. Nevertheless, the relative uncertainty of the highly populated bins is below 10% and can therefore be meaningfully interpreted.

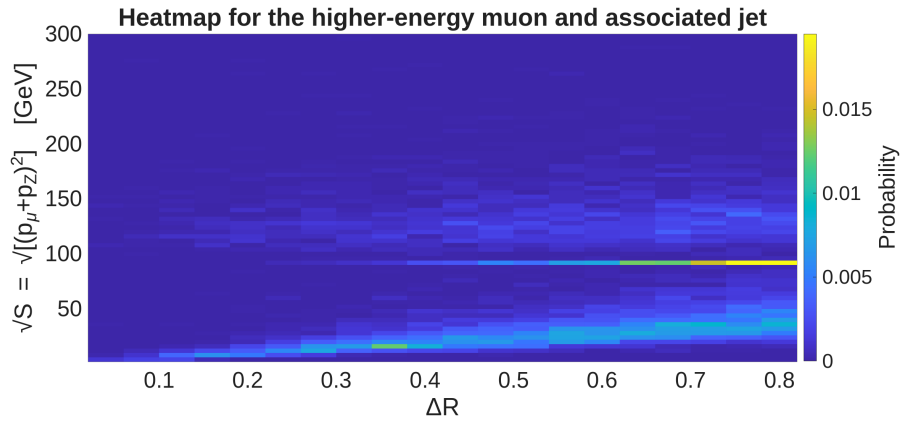


Figure 20: Globally normalized heatmap of $\Delta R$ as a function of $\sqrt{S}$ for the higher-energy muon and the associated jet in a sample of 50 000 events, shown for a cone radius of $R0 = 0.8$ with finer binning and a zoomed-in range.

As before, no clear sign of weak jets could be found, but other kinematic features could be observed. The most prominent feature in this graph is a sharp horizontal line at $\sqrt{S} \approx 90$ GeV. Since the mass of the Z boson is approximately 90 GeV [29], this could indicate a Z boson resonance. Above this line, at $\sqrt{S} \approx 125$ GeV, another accumulation of events is visible, although it is significantly more diffuse. This is approximately the mass of the Higgs boson [28] and could therefore be associated with Higgs production. The broad peak could be explained by the fact that not all decay products of the Higgs boson were captured in the constructed cone, as well as kinematic effects. Furthermore, there is an accumulation of events at $\sqrt{S} \lesssim 70$ GeV that could be explained by hadronic contributions captured within the cone.

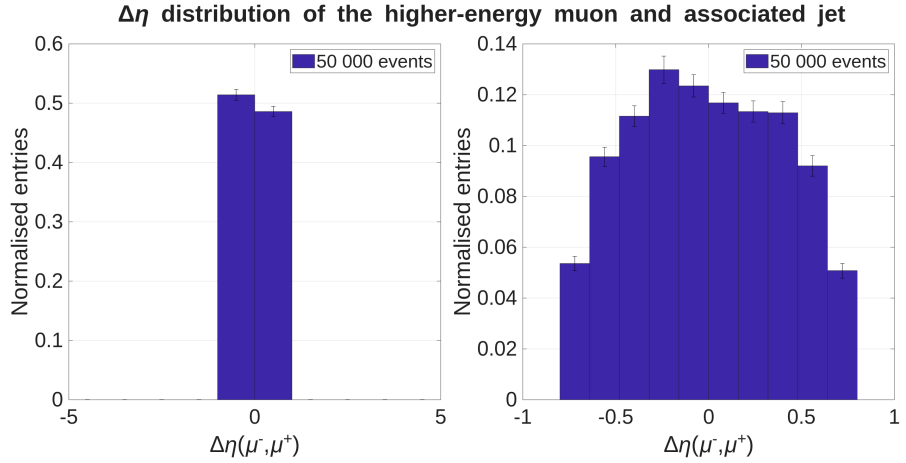


Figure 21: Distribution of the pseudorapidity difference $\Delta\eta$ for the higher-energy muon and the associated jet in a sample of 50 000 events. The left (right) panel shows the distribution with coarser binning (a zoomed-in view) for a cone radius of $R0 = 0.8$.

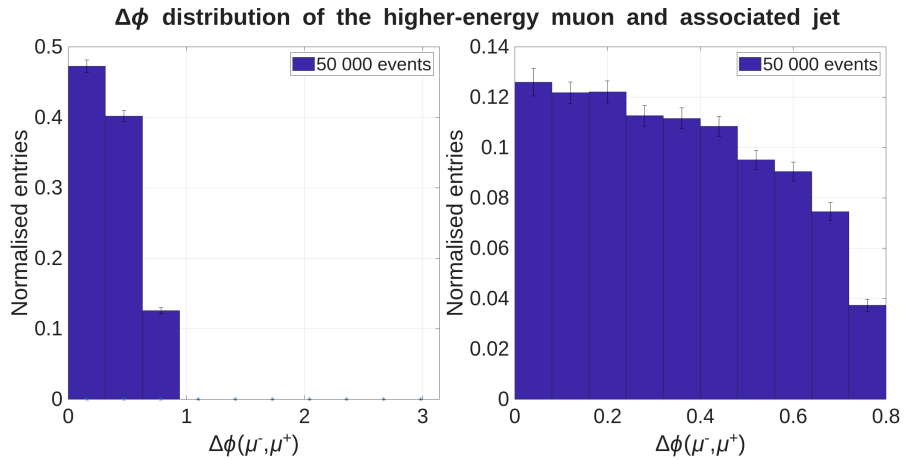


Figure 22: Distribution of the azimuthal angle difference $\Delta\phi$ for the higher-energy muon and the associated jet in a sample of 50 000 events. The left (right) panel shows a distribution with coarser binning (a zoomed-in view) for a cone radius of $R0 = 0.8$.

The $\Delta\eta$ and $\Delta\phi$ distributions were very similar to the distributions 15 and 16 in the previous section. Therefore, the same conclusions can be applied to this analysis.

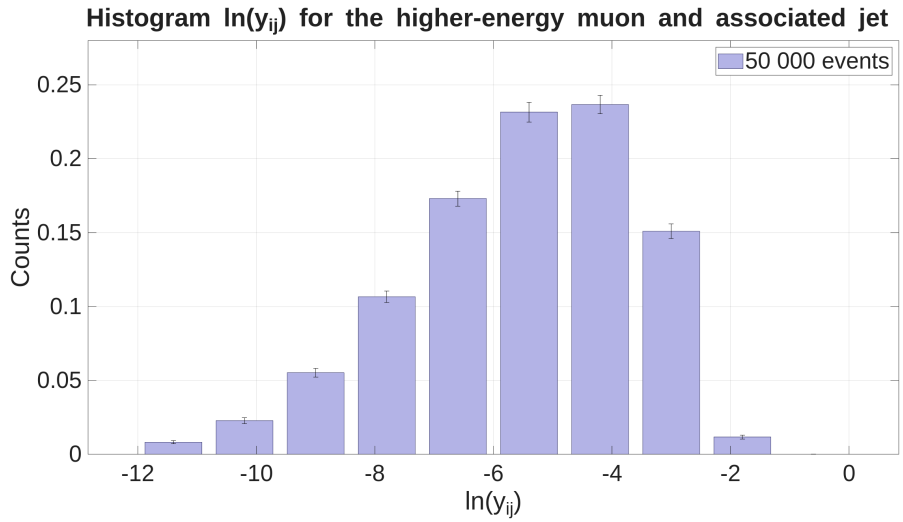


Figure 23: Logarithmic distribution of the Durham variable for the higher-energy muon and the associated jet in a sample of 50 000 events for a cone radius $R0 = 0.8$.

Compared to the previous section, this Durham distribution shows a shift of the peak toward larger values. Considering that the angular distributions remained fairly similar, this indicates that the energy asymmetry between the two objects decreased. In this case the relative energies between the constructed jet and the higher-energy muon seem to be more similar than between the higher-energy muon and the Z-cone jet.

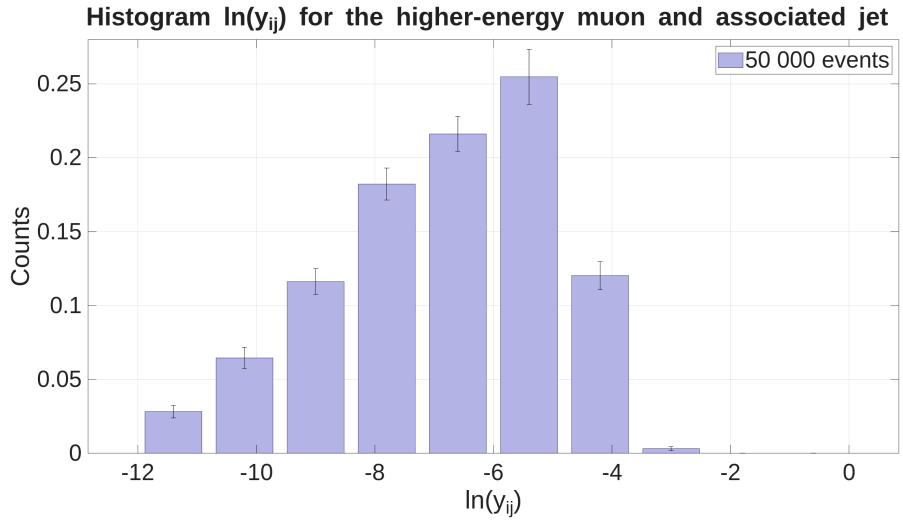


Figure 24: Logarithmic distribution of the Durham variable for the higher-energy muon and the associated jet in a sample of 50 000 events for a cone radius $R0 = 0.4$.

The same behavior could also be observed for the Durham distribution of the cone radius $R0 = 0.4$.

Taken together, these figures suggest that the jet and the higher-energy muon are collimated and have a lower energy asymmetry than in the previous analysis. There were also hints of Z boson and Higgs boson resonances detected, as well as hadronic contributions. Apart from this, no signs of weak jets could be detected in this analysis.

# 5. Summary

In this thesis, proton-proton collisions were studied with a focus on the process $pp \to \mu^-\mu^+jj$. The objective was to search for weak-jet signatures in this setup. To this end, it was simulated with `Herwig` and the resulting data were then analyzed by plotting different heatmaps, $\Delta\eta$ and $\Delta\phi$ distributions, as well as the corresponding Durham histograms. This analysis was performed for the following relations:

- muon-antimuon pair $(\mu^-, \mu^+)$
- muon and Z boson $(\mu^-, Z)$
- the higher-energy muon from the muon-antimuon pair and the Z boson $(\mu^-/\mu^+, Z)$
- a cone jet constructed around the higher-energy muon/antimuon filled with the Z boson $(\mu^-/\mu^+, Z_{cone})$
- a cone jet constructed around the higher-energy muon/antimuon containing all QCD particles within it $(\mu^-/\mu^+, jj)$

In all of these plots, no clear indication of weak jets could be found, but insights into the kinematic properties of these systems could be obtained.
For the muon-antimuon pair, it was observed that it was predominantly produced back-to-back and with similar pseudorapidities. A possible energy asymmetry was indicated. The muon-Z distributions suggested a correlation between $\Delta R$ and $\sqrt{S}$ as well as a tendency towards back-to-back behavior between the particles. Additionally, an energy asymmetry was observed, which was larger than in the previous analysis.
When considering the higher-energy muon-Z system, similar results were observed, with the difference that the higher-energy muon appears to be more strongly back-to-back correlated with the Z boson than the lower-energy one.
In the case of the constructed Z-cone jet compared to the higher-energy muon, the measured energies in the heatmaps were much smaller due to the limited cone radius. In a zoom of this structure an accumulation of events at approximately 125 GeV was observed, which may indicate the presence of a Higgs boson. Also the two objects appear to be highly collimated, as the cone was designed to select such events.
Finally, the relation between the higher-energy muon and the constructed cone jet, containing all QCD particles, was examined. The system also displays collimated behavior and a smaller energy asymmetry than the previous analysis. There were also hints of Z boson and Higgs boson resonances observed, as well as hadronic contributions.

# References

[1] J. Bleck-Neuhaus. *Elementare Teilchen*. Springer Spektrum, 2013. doi:10.1007/978-3-642-32579-3

[2] M. K. Gaillard, P. D. Grannis, F. J. Sciulli. *The standard model of particle physics. Reviews of Modern Physics*. Reviews of Modern Physics **71** (1999) 96. doi:10.1103/RevModPhys.71.S96

[3] I. J. R. Aitchison, A. J. Hey. *Gauge theories in particle physics : a practical introduction*. CRC Press, 2012. doi:10.1201/b13717

[4] H. Fritzsch, M. Gell-Mann, H. Leutwyler. *Advantages of the color octet gluon picture*. Physics Letters B **47** (1973) 365. doi:10.1016/0370-2693(73)90625-4

[5] G. Altarelli. *Collider Physics within the Standard Model A Primer*. Springer, 2017. doi:10.1007/978-3-319-51920-3_1

[6] A. Eichhorn. *An asymptotically safe guide to quantum gravity and matter*. Frontiers in Astronomy and Space Sciences **5** (2018). doi:10.3389/fspas.2018.00047

[7] D. H. Perkins. *Introduction to High Energy Physics*. Cambridge University Press, 2012. doi:10.1017/CBO9780511809040

[8] S. Marzani, G. Soyez, M. Spannowsky. *Looking Inside Jets*. Springer, 2019. doi:10.1007/978-3-030-15709-8

[9] J. M. Butterworth, G. Dissertori, G. P. Salam. *Hard Processes in Proton-Proton Collisions at the Large Hadron Collider*. Ann.Rev.Nucl.Part.Sci. **62** (2012) 387. doi:10.1146/annurev-nucl-102711-094913

[10] C. Patrignani, et al. (Particle Data Group). *Review of Particle Physics*. Chinese Physics C **40** (2016) 560. doi:10.1088/1674-1137/40/10/100001

[11] CMS, COLLABORATION. *Measurement of $B\overline{B}$ Angular Correlations based on Secondary Vertex Reconstruction at $\sqrt{s} = 7$ TeV.* Journal of High Energy Physics (2011).
doi:10.1007/JHEP03(2011)136

[12] S. NAVAS, ET AL. (PARTICLE DATA GROUP). *Review of Particle Physics.* Physics Review D **110** (2024) 781.
doi:10.1103/PhysRevD.110.030001

[13] S. D. ELLIS, C. K. VERMILION, J. R. WALSH, A. HORNIG, C. LEE. *Jet shapes and jet algorithms in SCET.* Journal of High Energy Physics **101** (2010) 2.
doi:10.1007/JHEP11(2010)101

[14] G. DISSERTORI, I. G. KNOWLES, M. SCHMELLING. *Quantum Chromodynamics - High Energy Experiments and Theory.* Oxford University Press, 2009.
doi:10.1093/acprof:oso/9780199566419.001.0001

[15] J. R. CHRISTIANSEN, T. SJOESTRAND. *Weak gauge boson radiation in parton showers.* Journal of High Energy Physics **115** (2014).
doi:10.1007/JHEP04(2014)115

[16] M. BÄHR, S. GIESEKE, M. A. GIGG, D. GRELLSCHEID, K. HAMILTON, O. LATUNDE-DADA, S. PLÄTZER, P. RICHARDSON, M. H. SEYMOUR, A. SHERSTNEV, B. R. WEBBER. *Herwig++ physics and manual.* The European Physical Journal C **58** (2008) 639–707.
doi:10.1140/epjc/s10052-008-0798-9

[17] G. CORCELLA, I. G. KNOWLES, G. MARCHESINI, S. MORETTI, K. ODAGIRI, P. RICHARDSON, M. H. SEYMOUR, B. R. WEBBER. *HERWIG 6: an event generator for hadron emission reactions with interfering gluons (including supersymmetric processes).* Journal of High Energy Physics (2001) 5.
doi:10.1088/1126-6708/2001/01/010

[18] S. GIESEKE, P. STEPHENS, B. WEBBER. *New formalism for QCD parton showers.* Journal of High Energy Physics **2003** (2004) 45.
doi:10.1088/1126-6708/2003/12/045

[19] J. BELLM, ET AL. *Herwig 7.0/7.1 Release Note.* European Physical Journal C **76** (2016) 196.
doi:10.1140/epjc/s10052-016-4018-8

[20] L. Lönnblad. *ThePEG: A Toolkit for High Energy Physics Event Generation.* Computer Physics Communications **118** (1999) 213.

[21] M. Bahr, et al. *Herwig++ Physics and Manual.* European Physical Journal C **58** (2008) 639.
doi:10.1140/epjc/s10052-008-0798-9

[22] J. Alwall, et al. *MadGraph 5: Going Beyond.* Journal of High Energy Physics **2011** (2011) 128.
doi:10.1007/JHEP06(2011)128

[23] S. Platzer, S. Gieseke. *Dipole Showers and Automated NLO Matching in Herwig++.* Journal of High Energy Physics **2011** (2011) 024.
doi:10.1007/JHEP01(2011)024

[24] M. Sjodahl. *ColorFull – a C++ library for calculations in SU(Nc) color space.* European Physical Journal C **75** (2015) 236.
doi:10.48550/arXiv.1412.3967

[25] R. Kleiss, et al. Electroweak Radiative Corrections. technical report CERN-89-08, CERN, 1989.

[26] H.-Y. Cheng, B. Tseng. *1/M corrections to baryonic form-factors in the quark model.* Physical Review D **53** (1996) 1457.
doi:10.1103/PhysRevD.53.1457

[27] H.-Y. Cheng. *Nonleptonic weak decays of bottom baryons.* Physical Review D **56** (1997) 2799.
doi:10.1103/PhysRevD.56.2799

[28] ATLAS and CMS Collaborations. *Combined Measurement of the Higgs Boson Mass.* Physical Review Letters **114** (2015) 191803.
doi:10.1103/PhysRevLett.114.191803

[29] ALEPH Collaboration, DELPHI Collaboration, L3 Collaboration, OPAL Collaboration, SLD Collaboration, LEP Electroweak Working Group, SLD Electroweak and Heavy Flavour Groups. *Precision Electroweak Measurements on the Z Resonance.* Physics Reports **427** (2006) 257–454.
doi:10.1016/j.physrep.2005.12.006

# List of Figures

# A. Code

Listing 1: **Rivet analysis code for** ($\mu^+\mu^-$)

```
//TTBAR02_mu_mu.cc
// -*- C++ -*-
#include "Rivet/Analysis.hh"
#include "Rivet/Projections/FinalState.hh"
#include "Rivet/Projections/IdentifiedFinalState.hh"

#include "Rivet/Tools/Cuts.hh"      // for cuts
#include "Rivet/Math/Units.hh"      // for GeV
#include <cmath>                    // for M_PI
#include "Rivet/Math/MathUtils.hh"  // for sqr


namespace Rivet {


  /// @brief Add a short analysis description here
  class TTBAR02 : public Analysis {
  public:

    /// Constructor
    DEFAULT_RIVET_ANALYSIS_CTOR(TTBAR02);


    /// @name Analysis methods

    /// Book histograms and initialize projections before the run
    void init() {

            // Initialize and register projections
        const FinalState fs;
        declare(fs, "FS");
        declare(IdentifiedFinalState(fs,13),"T"); // take all muons out of FS
        declare(IdentifiedFinalState(fs,-13),"TBAR"); // take all anti-muons out of FS

        // Book histograms
        // T... muon, _TBAR... antimuon, TTBAR... both
```

```
    // pT - Transverse momentum distribution
    book(_Hist_pT_T,"pT_T",nbins,0,1000);
    book( _Hist_pT_TBAR,"pT_TBAR",nbins,0,1000);
    book(_Hist_pT_TTBAR,"pT_TTBAR",nbins,0,1000);
    book(_Hist_PT_TTBAR,"PT_TTBAR",nbins,0,1000);

    // eta - pseudorapidity
    book(_Hist_eta_T,"eta_T",nbins,-max_eta,max_eta);
    book( _Hist_eta_TBAR,"eta_TBAR",nbins,-max_eta,max_eta);
    book(_Hist_eta_T_TBAR,"eta_T_TBAR",nbins,-2*max_eta,2*max_eta);

    // phi - azimuthal angle
    book(_Hist_phi_T,"phi_T",nbins,-M_PI,M_PI);
    book(_Hist_phi_TBAR,"phi_TBAR",nbins,-M_PI,M_PI);
    book(_Hist_phi_T_TBAR,"phi_T_TBAR",nbins,0,M_PI);

    // invariant mass
    book(_Hist_inv_T,"inv_T",nbins,0,200);
    book(_Hist_inv_TBAR,"inv_TBAR",nbins,0,200);
    book(_Hist_inv_TTBAR,"inv_TTBAR",nbins,0,2000);

    // DeltaR distribution
    book(_Hist_dR_T_TBAR, "dR_T_TBAR", nbins, 0, 6);

    // Durham distribution
    book(_Hist_Durham,"Durham",nbins,-12.0,0.0);
}


/// Perform the per-event analysis
void analyze(const Event& event)
{

    const double weight = event.weight();

    const auto& mus  = apply<IdentifiedFinalState>(event, "T").particlesByPt();
    const auto& amus = apply<IdentifiedFinalState>(event, "TBAR").particlesByPt();

    if (mus.empty() || amus.empty()) return; // return if no muon

    const Particle& TOP    = mus.front();    // muon
```

```
const Particle& TOPBAR = amus.front();   // antimuon

// Muon
const double pT_T  = TOP.pT();
const double eta_T = TOP.eta();
const double phi_T = TOP.phi();
const FourMomentum P_T = TOP.mom();

_Hist_pT_T  -> fill(pT_T,  weight);
_Hist_eta_T -> fill(eta_T, weight);
_Hist_phi_T -> fill(phi_T, weight);
_Hist_inv_T -> fill(P_T.mass(), weight);

// Antimuon
const double pT_TBAR  = TOPBAR.pT();
const double eta_TBAR = TOPBAR.eta();
const double phi_TBAR = TOPBAR.phi();
const FourMomentum P_TBAR = TOPBAR.mom();

_Hist_pT_TBAR  -> fill(pT_TBAR,  weight);
_Hist_eta_TBAR -> fill(eta_TBAR, weight);
_Hist_phi_TBAR -> fill(phi_TBAR, weight);
_Hist_inv_TBAR -> fill(P_TBAR.mass(), weight);

// Muon - Antimuon
const FourMomentum P_TTBAR = P_T + P_TBAR;
_Hist_phi_T_TBAR -> fill(deltaPhi(phi_T, phi_TBAR), weight);
_Hist_eta_T_TBAR -> fill(eta_T - eta_TBAR, weight);
_Hist_inv_TTBAR  -> fill(P_TTBAR.mass(), weight);
_Hist_pT_TTBAR   -> fill((pT_T + pT_TBAR), weight);
_Hist_PT_TTBAR   -> fill(P_TTBAR.pT(), weight);



// DeltaR distribution
const double dphi = deltaPhi(phi_T, phi_TBAR);
const double deta = (eta_T - eta_TBAR);
const double dR   = sqrt(sqr(deta) + sqr(dphi));
if (std::isfinite(dR)) _Hist_dR_T_TBAR->fill(dR, weight);
```

```
    // Durham distribution

    // Measure Energies E_i,E_j
    double E_i = P_T.E();
    double E_j = P_TBAR.E();
    // Angle between a muon - antimuon pair
    double cosTheta = cos(P_T.angle(P_TBAR));
    cosTheta = std::max(-1.0, std::min(1.0, cosTheta)); // avoid rounding errors
    double E_s = sqr(E_i + E_j);
    if (E_s > 0 && std::isfinite(E_s)) {
      // Formula for the durham algorithm
      double y_ij = (2.0*sqr(std::min(E_i, E_j)) / E_s) * (1.0-cosTheta);
      if (y_ij > 0 && std::isfinite(y_ij)) {
        _Hist_Durham-> fill(std::log(y_ij),weight);
      }
    }
}


/// Normalize histograms etc., after the run
void finalize()
{
    // pT - Histograms for T,TBAR,TTBAR
    normalize(_Hist_pT_T);
    normalize(_Hist_pT_TBAR);
    normalize(_Hist_pT_TTBAR);
    normalize(_Hist_PT_TTBAR);

    // eta - Histograms for T,TBAR,T_TBAR
    normalize(_Hist_eta_T);
    normalize(_Hist_eta_TBAR);
    normalize(_Hist_eta_T_TBAR);

    // phi - Histograms for T,TBAR,T_TBAR
    normalize(_Hist_phi_T);
    normalize(_Hist_phi_TBAR);
    normalize(_Hist_phi_T_TBAR);

    // invariant mass - Histograms for T,TBAR,T_TBAR
    normalize(_Hist_inv_T);
    normalize(_Hist_inv_TBAR);
```

```
    normalize(_Hist_inv_TTBAR);

    // DeltaR distribution
    normalize(_Hist_dR_T_TBAR);

    // Durham distribution
    normalize(_Hist_Durham);
}

private:

double max_eta = 5.;    // accelerator max eta
    int nbins = 10;         // number of bins

    // Histogram pointers

    // pT
    Histo1DPtr _Hist_pT_T;
    Histo1DPtr _Hist_pT_TBAR;
    Histo1DPtr _Hist_pT_TTBAR;
    Histo1DPtr _Hist_PT_TTBAR;

    // eta
    Histo1DPtr _Hist_eta_T;
    Histo1DPtr _Hist_eta_TBAR;
    Histo1DPtr _Hist_eta_T_TBAR;

    // phi
    Histo1DPtr _Hist_phi_T;
    Histo1DPtr _Hist_phi_TBAR;
    Histo1DPtr _Hist_phi_T_TBAR;

    // invariant mass
    Histo1DPtr _Hist_inv_T;
    Histo1DPtr _Hist_inv_TBAR;
    Histo1DPtr _Hist_inv_TTBAR;

    // DeltaR distribution
    Histo1DPtr _Hist_dR_T_TBAR;

    // Durham distribution
```

```
    Histo1DPtr _Hist_Durham;

  };


  // The hook for the plugin system
  DECLARE_RIVET_PLUGIN(TTBAR02);


}
```

Listing 2: **Rivet analysis code for** ($\mu^-$ Z)

```
//TTBAR02_mu_Z.cc
// -*- C++ -*-
#include "Rivet/Analysis.hh"
#include "Rivet/Projections/FinalState.hh"
#include "Rivet/Projections/IdentifiedFinalState.hh"

#include "Rivet/Tools/Cuts.hh"      // for Cuts
#include "Rivet/Math/Units.hh"      // for GeV
#include <cmath>                    // for M_PI
#include "Rivet/Math/MathUtils.hh"  // for sqr
#include <algorithm>                // for std::min

namespace Rivet {

  /// @brief Add a short analysis description here
  class TTBAR02 : public Analysis {
  public:

    /// Constructor
    DEFAULT_RIVET_ANALYSIS_CTOR(TTBAR02);

    /// @name Analysis methods

    /// Book histograms and initialize projections before the run
    void init() {

        // Initialize and register projections
        const FinalState fs;
        declare(fs, "FS");
```

```
    declare(IdentifiedFinalState(fs,13),"T");
    declare(IdentifiedFinalState(fs, 23), "Z");

    // Book histograms
    // T... muon, Z... Z-boson

    // pT - Transverse momentum distribution
    book(_Hist_pT_T,"pT_T",nbins,0,1000);

    // eta - pseudorapidity
    book(_Hist_eta_T,"eta_T",nbins,-max_eta,max_eta);
    book(_Hist_eta_Z,"eta_Z",nbins,-max_eta,max_eta);
    // delta eta (muon vs Z)
    book(_Hist_delta_eta,"delta_eta",nbins,-max_deta,max_deta);

    // phi - azimuthal angle
    book(_Hist_phi_T,"phi_T",nbins,-M_PI,M_PI);
    book(_Hist_phi_Z,"phi_Z",nbins,-M_PI,M_PI);
    // delta phi (muon vs Z)
    book(_Hist_delta_phi,"delta_phi",nbins,0,M_PI);


    // invariant mass
    book(_Hist_inv_T,"inv_T",nbins,0,200);
    book(_Hist_inv_Z,"inv_Z",nbins,0,200);

    // DeltaR distribution muon vs Z
    book(_Hist_dR_T_Z, "dR_T_Z", nbins, 0, 6);


    // sqrtS - invariant mass of the combined muon-Z-system
    book(_Hist_S_T_Z, "S_T_Z", nbins, 0, 500);

    // Heatmap DeltaR vs sqrtS
    book(_Hist_Lego_T_Z, "lego_T_Z",nbins, 0, 6,nbins, 0, 500);

    // Durham distribution muon vs Z
    book(_Hist_Durham,"Durham",nbins,-12.0,0.0);
}
```

```
/// Perform the per-event analysis
void analyze(const Event& event)
{
    const double weight = event.weight();

    const auto& mus  = apply<IdentifiedFinalState>(event, "T").particlesByPt();
    const auto& Zs = apply<IdentifiedFinalState>(event, "Z").particlesByPt();

    if (mus.empty()) return; // return if no muon
    if (Zs.empty()) return; // return if no Z

    const Particle& TOP    = mus.front();     // muon
    const Particle& Z = Zs.front();           // Z

    // Muon
    const double pT_T  = TOP.pT();
    const double eta_T = TOP.eta();
    const double phi_T = TOP.phi();
    const FourMomentum P_T = TOP.mom();

    _Hist_pT_T  -> fill(pT_T,  weight);
    _Hist_eta_T -> fill(eta_T, weight);
    _Hist_phi_T -> fill(phi_T, weight);
    _Hist_inv_T -> fill(P_T.mass(), weight);

    // Z-boson
    const double eta_Z = Z.eta();
    const double phi_Z = Z.phi();
    const FourMomentum P_Z = Z.mom();

    _Hist_eta_Z -> fill(eta_Z, weight);
    _Hist_phi_Z -> fill(phi_Z, weight);
    _Hist_inv_Z -> fill(P_Z.mass(), weight);



    // DeltaR distribution for muon vs Z
    const double dphi = deltaPhi(phi_T, phi_Z);
    const double deta = (eta_T - eta_Z);
    const double dR   = sqrt(sqr(deta) + sqr(dphi));
    if (std::isfinite(dR)) _Hist_dR_T_Z->fill(dR, weight);
```

```
    _Hist_delta_phi -> fill(dphi,weight);
    _Hist_delta_eta -> fill(deta, weight);


    // sqrtS - invariant mass of the combined muon-Z-system
    const double sqrtS = (P_T + P_Z).mass();
    _Hist_S_T_Z -> fill(sqrtS, weight);

    // Heatmap DeltaR vs sqrtS
    _Hist_Lego_T_Z -> fill(dR,sqrtS,weight);


    // Durham distribution

    // Measure Energies E_i,E_j
    double E_i = P_T.E(); // muon
    double E_j = P_Z.E(); // Z
    // Angle between muon and Z boson
    double cosTheta = cos(P_T.angle(P_Z));
    cosTheta = std::max(-1.0, std::min(1.0, cosTheta)); // avoid rounding errors
    double E_s = sqr(E_i + E_j);
    if (E_s > 0 && std::isfinite(E_s)) {
      // Formula for the durham algorithm
      double y_ij = (2.0*sqr(std::min(E_i, E_j)) / E_s) * (1.0-cosTheta);
      if (y_ij > 0 && std::isfinite(y_ij)) {
        _Hist_Durham-> fill(std::log(y_ij),weight);
      }
    }
}

/// Normalize histograms etc., after the run
void finalize()
{
    // pT - Histograms for T
    normalize(_Hist_pT_T);

    // eta - Histograms for T, Z
    normalize(_Hist_eta_T);
    normalize(_Hist_eta_Z);
    normalize(_Hist_delta_eta);
```

```
      // phi - Histograms for T, Z
      normalize(_Hist_phi_T);
      normalize(_Hist_phi_Z);
      normalize(_Hist_delta_phi);

      // invariant mass - Histograms for T, Z
      normalize(_Hist_inv_T);
      normalize(_Hist_inv_Z);

      // DeltaR distribution muon vs Z
      normalize(_Hist_dR_T_Z);

      // sqrtS
      normalize(_Hist_S_T_Z);

      // Durham distribution
      normalize(_Hist_Durham);


  }

private:

  double max_eta = 5.;
  double max_deta = 10.;
  int nbins = 10;

  // Histogram pointers

      // pT - Histograms for T, Z
      Histo1DPtr _Hist_pT_T;

      // eta - Histograms for T, Z
      Histo1DPtr _Hist_eta_T;
      Histo1DPtr _Hist_eta_Z;
      Histo1DPtr _Hist_delta_eta;

      // phi - Histograms for T, Z
      Histo1DPtr _Hist_phi_T;
      Histo1DPtr _Hist_phi_Z;
      Histo1DPtr _Hist_delta_phi;
```

```
    // invariant mass - Histograms for T, Z
    Histo1DPtr _Hist_inv_T;
    Histo1DPtr _Hist_inv_Z;

    // DeltaR distribution for muon vs Z
    Histo1DPtr _Hist_dR_T_Z;

    // sqrtS
    Histo1DPtr _Hist_S_T_Z;

    // Heatmap DeltaR vs sqrtS
    Histo2DPtr _Hist_Lego_T_Z;

    // y_ij Durham
    Histo1DPtr _Hist_Durham;

  };

  // The hook for the plugin system
  DECLARE_RIVET_PLUGIN(TTBAR02);

}
```

Listing 3: **Rivet analysis code for** (higher-energy $\mu$ vs Z)

```
//TTBAR02_higher_energy_mu_Z.cc
// -*- C++ -*-
#include "Rivet/Analysis.hh"
#include "Rivet/Projections/FinalState.hh"
#include "Rivet/Projections/IdentifiedFinalState.hh"

#include "Rivet/Tools/Cuts.hh"      // for Cuts
#include "Rivet/Math/Units.hh"      // for GeV
#include <cmath>                    // for M_PI
#include "Rivet/Math/MathUtils.hh"  // for sqr
#include <algorithm>                // for std::min

namespace Rivet {

  /// @brief Add a short analysis description here
  class TTBAR02 : public Analysis {
```

```
public:

  /// Constructor
  DEFAULT_RIVET_ANALYSIS_CTOR(TTBAR02);

  /// @name Analysis methods

  /// Book histograms and initialize projections before the run
  void init() {

      // Initialize and register projections
      const FinalState fs;
      declare(fs, "FS");
      declare(IdentifiedFinalState(fs,13),"T");
      declare(IdentifiedFinalState(fs,-13),"TBAR");
      declare(IdentifiedFinalState(fs, 23), "Z");

      // Book histograms
      // T... muon, _TBAR... antimuon, TTBAR... both, Z... Z-boson

      // pT - Transverse momentum distribution
      book(_Hist_pT_T,"pT_T",nbins,0,1000);
      book( _Hist_pT_TBAR,"pT_TBAR",nbins,0,1000);

      // eta - pseudorapidity
      book(_Hist_eta_T,"eta_T",nbins,-max_eta,max_eta);
      book( _Hist_eta_TBAR,"eta_TBAR",nbins,-max_eta,max_eta);
      book( _Hist_eta_Z,"eta_Z",nbins,-max_eta,max_eta);
      book( _Hist_deta,"deta",nbins,-2*max_eta,2*max_eta);

      // phi - azimuthal angle
      book(_Hist_phi_T,"phi_T",nbins,-M_PI,M_PI);
      book(_Hist_phi_TBAR,"phi_TBAR",nbins,-M_PI,M_PI);
      book(_Hist_phi_Z,"phi_Z",nbins,-M_PI,M_PI);
      book(_Hist_dphi,"dphi",nbins,0,M_PI);

      // invariant mass
      book(_Hist_inv_T,"inv_T",nbins,0,200);
      book(_Hist_inv_TBAR,"inv_TBAR",nbins,0,200);
      book(_Hist_inv_Z,"inv_Z",nbins,0,200);
```

```
    // DeltaR distribution for (muon or antimuon) vs Z
    book(_Hist_dR_T_Z, "dR_T_Z", nbins, 0, 6);

    // sqrtS - invariant mass of the combined muon-Z-system
    book(_Hist_S_T_Z, "S_T_Z", nbins, 0, 500);

    // Heatmap DeltaR vs sqrtS
    book(_Hist_Lego_T_Z, "lego_T_Z",nbins, 0, 6,nbins, 0, 500);

    // Durham distribution for (muon or antimuon) vs Z
    book(_Hist_Durham,"Durham",nbins,-12.0,0.0);

}


/// Perform the per-event analysis
void analyze(const Event& event)
{
    const double weight = event.weight();

    const auto& mus  = apply<IdentifiedFinalState>(event, "T").particlesByPt();
    const auto& amus = apply<IdentifiedFinalState>(event, "TBAR").particlesByPt();
    const auto& Zs = apply<IdentifiedFinalState>(event, "Z").particlesByPt();  // Z

    if (mus.empty() || amus.empty()) return; // return if no muon
    if (Zs.empty()) return; // return if no Z

    const Particle& TOP    = mus.front();    // muon
    const Particle& TOPBAR = amus.front();   // antimuon
    const Particle& Z = Zs.front();          //Z

    // Muon
    const double pT_T  = TOP.pT();
    const double eta_T = TOP.eta();
    const double phi_T = TOP.phi();
    const FourMomentum P_T = TOP.mom();

    _Hist_pT_T  -> fill(pT_T,  weight);
    _Hist_eta_T -> fill(eta_T, weight);
    _Hist_phi_T -> fill(phi_T, weight);
```

```
_Hist_inv_T -> fill(P_T.mass(), weight);

// Anti-Muon
const double pT_TBAR  = TOPBAR.pT();
const double eta_TBAR = TOPBAR.eta();
const double phi_TBAR = TOPBAR.phi();
const FourMomentum P_TBAR = TOPBAR.mom();

_Hist_pT_TBAR  -> fill(pT_TBAR,  weight);
_Hist_eta_TBAR -> fill(eta_TBAR, weight);
_Hist_phi_TBAR -> fill(phi_TBAR, weight);
_Hist_inv_TBAR -> fill(P_TBAR.mass(), weight);

// Z-boson
const double eta_Z = Z.eta();
const double phi_Z = Z.phi();
const FourMomentum P_Z = Z.mom();

_Hist_eta_Z -> fill(eta_Z, weight);
_Hist_phi_Z -> fill(phi_Z, weight);
_Hist_inv_Z -> fill(P_Z.mass(), weight);


// choosing the higher energy muon or antimuon
const bool takeT = (P_T.E() > P_TBAR.E()) || (P_T.E() == P_TBAR.E() && pT_T >= pT_TBAR);
// kinematics of the higher energy particle
const FourMomentum& P_MU = takeT ? P_T : P_TBAR;
const double eta_MU = takeT ? eta_T : eta_TBAR;
const double phi_MU = takeT ? phi_T : phi_TBAR;


// DeltaR distribution for (muon or antimuon) vs Z
const double dphi = deltaPhi(phi_MU, phi_Z);
const double deta = (eta_MU - eta_Z);
const double dR  = sqrt(sqr(deta) + sqr(dphi));
_Hist_dphi -> fill(dphi, weight);
_Hist_deta -> fill(deta, weight);
if (std::isfinite(dR)) _Hist_dR_T_Z->fill(dR, weight);


// sqrtS - invariant mass of the combined muon-Z-system
```

```
    const double sqrtS = (P_MU + P_Z).mass();
    _Hist_S_T_Z -> fill(sqrtS, weight);


    // Heatmap DeltaR vs sqrtS
    _Hist_Lego_T_Z -> fill(dR,sqrtS,weight);


    // Durham distribution

    // Measure Energies E_i,E_j
    const double E_j = P_Z.E(); // Z
    const double E_i = P_MU.E(); //( or )
    // Angle between higher energy muon/antimuon and Z-boson
    double cosTheta = cos(P_MU.angle(P_Z));
    cosTheta = std::max(-1.0, std::min(1.0, cosTheta)); // avoid rounding errors
    const double E_s = sqr(E_i + E_j);
    if (E_s > 0 && std::isfinite(E_s)) {
      // Formula for the durham algorithm
      const double y_ij = (2.0*sqr(std::min(E_i, E_j)) / E_s) * (1.0-cosTheta);
      if (y_ij > 0 && std::isfinite(y_ij)) {
       _Hist_Durham-> fill(std::log(y_ij),weight);
      }
    }
}



/// Normalize histograms etc., after the run
void finalize()
{
    // pT - Histograms for T,TBAR
    normalize(_Hist_pT_T);
    normalize(_Hist_pT_TBAR);

    // eta - Histograms for T,TBAR,Z
    normalize(_Hist_eta_T);
    normalize(_Hist_eta_TBAR);
    normalize(_Hist_eta_Z);
    normalize(_Hist_deta);
```

```
    // phi - Histograms for T,TBAR,Z
    normalize(_Hist_phi_T);
    normalize(_Hist_phi_TBAR);
    normalize(_Hist_phi_Z);
    normalize(_Hist_dphi);

    // invariant mass - Histograms for T,TBAR,Z
    normalize(_Hist_inv_T);
    normalize(_Hist_inv_TBAR);
    normalize(_Hist_inv_Z);

    // DeltaR distribution for ( or ) vs Z
    normalize(_Hist_dR_T_Z);

    // sqrtS - invariant mass of the combined muon-Z-system
    normalize(_Hist_S_T_Z);

    // Durham distribution
    normalize(_Hist_Durham);


  }

private:

  double max_eta = 5.; // accelerator max eta
  int nbins = 10; // number of bins

    // Histogram pointers

    // pT
    Histo1DPtr _Hist_pT_T;
    Histo1DPtr _Hist_pT_TBAR;

    // eta
    Histo1DPtr _Hist_eta_T;
    Histo1DPtr _Hist_eta_TBAR;
    Histo1DPtr _Hist_eta_Z;
    Histo1DPtr _Hist_deta;

    // phi
```

```
    Histo1DPtr _Hist_phi_T;
    Histo1DPtr _Hist_phi_TBAR;
    Histo1DPtr _Hist_phi_Z;
    Histo1DPtr _Hist_dphi;

    // invariant mass
    Histo1DPtr _Hist_inv_T;
    Histo1DPtr _Hist_inv_TBAR;
    Histo1DPtr _Hist_inv_Z;

    // DeltaR distribution
    Histo1DPtr _Hist_dR_T_Z;

    // sqrtS
    Histo1DPtr _Hist_S_T_Z;

    // Heatmap DeltaR vs sqrtS
    Histo2DPtr _Hist_Lego_T_Z;

    // Durham distribution
    Histo1DPtr _Hist_Durham;

  };

  // The hook for the plugin system
  DECLARE_RIVET_PLUGIN(TTBAR02);

}
```

Listing 4: **Rivet analysis code for** (higher-energy $\mu$ vs Z cone jet)

```
//TTBAR02_Z_cone.cc
// -*- C++ -*-
#include "Rivet/Analysis.hh"
#include "Rivet/Projections/FinalState.hh"
#include "Rivet/Projections/IdentifiedFinalState.hh"

#include "Rivet/Tools/Cuts.hh"      // for Cuts
#include "Rivet/Math/Units.hh"      // for GeV
#include <cmath>                    // for M_PI
#include "Rivet/Math/MathUtils.hh"  // for sqr
#include <algorithm>                // for std::min
```

```
namespace Rivet {

  /// @brief Add a short analysis description here
  class TTBAR02 : public Analysis {
  public:

    /// Constructor
    DEFAULT_RIVET_ANALYSIS_CTOR(TTBAR02);

    /// @name Analysis methods

    /// Book histograms and initialize projections before the run
    void init() {

        // Initialize and register projections
        const FinalState fs;
        declare(fs, "FS");
        declare(IdentifiedFinalState(fs,13),"T");
        declare(IdentifiedFinalState(fs,-13),"TBAR");
        declare(IdentifiedFinalState(fs, 23), "Z");

        // Book histograms
        // T... muon, _TBAR... antimuon, TTBAR... both, Z... Z-boson

        // pT - Transverse momentum distribution
        book(_Hist_pT_T,"pT_T",nbins,0,1000);
        book( _Hist_pT_TBAR,"pT_TBAR",nbins,0,1000);

        // eta - pseudorapidity
        book(_Hist_eta_T,"eta_T",nbins,-max_eta,max_eta);
        book( _Hist_eta_TBAR,"eta_TBAR",nbins,-max_eta,max_eta);
        book( _Hist_eta_Z,"eta_Z",nbins,-max_eta,max_eta);
        // delta eta (muon vs Z cone)
        // book(_Hist_deta,"deta",nbins,-5,5);
        book(_Hist_deta,"deta",nbins,-0.8,0.8);

        // phi - azimuthal angle
        book(_Hist_phi_T,"phi_T",nbins,-M_PI,M_PI);
        book(_Hist_phi_TBAR,"phi_TBAR",nbins,-M_PI,M_PI);
        book(_Hist_phi_Z,"phi_Z",nbins,-M_PI,M_PI);
```

```
    // delta phi (muon vs Z cone)
    // book(_Hist_dphi,"dphi",nbins,0,M_PI);
    book(_Hist_dphi,"dphi",nbins,0,0.8);

    // invariant mass
    book(_Hist_inv_T,"inv_T",nbins,0,200);
    book(_Hist_inv_TBAR,"inv_TBAR",nbins,0,200);
    book(_Hist_inv_Z,"inv_Z",nbins,0,200);


    // DeltaR distribution for (muon or antimuon) vs Z cone jet
    book(_Hist_dR_T_Z_cone, "dR_T_Z_cone", nbins, 0, 6);

    // sqrtS - invariant mass of the combined muon-Z-system
    book(_Hist_S_T_Z_cone, "S_T_Z_cone", nbins, 0, 500);

    // Heatmap DeltaR vs sqrtS
    book(_Hist_Lego_T_Z_cone, "lego_T_Z",nbins, 0, 6,nbins, 0, 500);

    // Durham distribution for (muon or antimuon) vs Z cone jet
    book(_Hist_Durham,"Durham",nbins,-12.0,0.0);
}


/// Perform the per-event analysis
void analyze(const Event& event)
{
  const double weight = event.weight();

  const auto& mus  = apply<IdentifiedFinalState>(event, "T").particlesByPt();
  const auto& amus = apply<IdentifiedFinalState>(event, "TBAR").particlesByPt();
  const auto& Zs = apply<IdentifiedFinalState>(event, "Z").particlesByPt();  //Z

  if (mus.empty() || amus.empty()) return; // return if no muon
  if (Zs.empty()) return; // return if no Z

  const double R0 = 0.8; // Cone-radius

  const Particle& TOP    = mus.front();    // muon
  const Particle& TOPBAR = amus.front();   // antimuon
  const Particle& Z = Zs.front();          // Z
```

```
// Muon
const double pT_T  = TOP.pT();
const double eta_T = TOP.eta();
const double phi_T = TOP.phi();
const FourMomentum P_T = TOP.mom();

_Hist_pT_T  -> fill(pT_T,  weight);
_Hist_eta_T -> fill(eta_T, weight);
_Hist_phi_T -> fill(phi_T, weight);
_Hist_inv_T -> fill(P_T.mass(), weight);

// Anti-Muon
const double pT_TBAR  = TOPBAR.pT();
const double eta_TBAR = TOPBAR.eta();
const double phi_TBAR = TOPBAR.phi();
const FourMomentum P_TBAR = TOPBAR.mom();

_Hist_pT_TBAR  -> fill(pT_TBAR,  weight);
_Hist_eta_TBAR -> fill(eta_TBAR, weight);
_Hist_phi_TBAR -> fill(phi_TBAR, weight);
_Hist_inv_TBAR -> fill(P_TBAR.mass(), weight);

// Z-boson
const double eta_Z = Z.eta();
const double phi_Z = Z.phi();
const FourMomentum P_Z = Z.mom();

_Hist_eta_Z -> fill(eta_Z, weight);
_Hist_phi_Z -> fill(phi_Z, weight);
_Hist_inv_Z -> fill(P_Z.mass(), weight);

// choosing the higher energy muon or antimuon
const bool takeT = (P_T.E() > P_TBAR.E()) || (P_T.E() == P_TBAR.E() && pT_T >= pT_TBAR);
// kinematics of the higher energy particle
const FourMomentum& P_MU = takeT ? P_T : P_TBAR;
const double eta_MU = takeT ? eta_T : eta_TBAR;
const double phi_MU = takeT ? phi_T : phi_TBAR;
```

```
FourMomentum P_cone;

// calculate the Z cone
for (const Particle& Zcone : Zs) {
  const double dphi_mu_Z = deltaPhi(phi_MU, Zcone.phi());
  const double dR_mu_Z = sqrt( sqr(eta_MU - Zcone.eta()) + sqr(dphi_mu_Z) );
  if (dR_mu_Z < R0) {
    P_cone += Zcone.mom();
  }
}
if (P_cone.E() <= 0) return;

// Kinematics of the Z cone
const double eta_cone = P_cone.eta();
const double phi_cone = P_cone.phi();

// DeltaR distribution for (muon or antimuon) vs Z cone jet
const double dphi = deltaPhi(phi_MU, phi_cone);
const double deta = (eta_MU - eta_cone);
const double dR  = sqrt(sqr(deta) + sqr(dphi));
_Hist_dphi -> fill(dphi, weight);
_Hist_deta -> fill(deta, weight);
if (std::isfinite(dR)) _Hist_dR_T_Z_cone -> fill(dR, weight);

// sqrtS - invariant mass of the combined muon-Z-system
const double sqrtS = (P_MU + P_cone).mass();
_Hist_S_T_Z_cone -> fill(sqrtS, weight);

// Heatmap DeltaR vs sqrtS
_Hist_Lego_T_Z_cone -> fill(dR,sqrtS,weight);


// Durham distribution

// Measure Energies E_i,E_j
const double E_j = P_cone.E();
const double E_i = P_MU.E();
// Angle between higher energy muon/antimuon and Z cone jet
double cosTheta = cos(P_MU.angle(P_cone));
cosTheta = std::max(-1.0, std::min(1.0, cosTheta)); // avoid rounding errors
const double E_s = sqr(E_i + E_j);
```

```
    if (E_s > 0 && std::isfinite(E_s)) {
      // Formula for the durham algorithm
      const double y_ij = (2.0*sqr(std::min(E_i, E_j)) / E_s) * (1.0-cosTheta);
      if (y_ij > 0 && std::isfinite(y_ij)) {
       _Hist_Durham-> fill(std::log(y_ij),weight);
      }
    }
}


/// Normalize histograms etc., after the run
void finalize()
{
    // pT - Histograms for T,TBAR
    normalize(_Hist_pT_T);
    normalize(_Hist_pT_TBAR);

    // eta - Histograms for T,TBAR,Z
    normalize(_Hist_eta_T);
    normalize(_Hist_eta_TBAR);
    normalize(_Hist_eta_Z);
    normalize(_Hist_deta);

    // phi - Histograms for T,TBAR,Z
    normalize(_Hist_phi_T);
    normalize(_Hist_phi_TBAR);
    normalize(_Hist_phi_Z);
    normalize(_Hist_dphi);

    // invariant mass - Histograms for T,TBAR,Z
    normalize(_Hist_inv_T);
    normalize(_Hist_inv_TBAR);
    normalize(_Hist_inv_Z);

    // DeltaR distribution for (muon or antimuon) vs Z cone jet
    normalize(_Hist_dR_T_Z_cone);

    // sqrtS - invariant mass of the combined muon-Z(jet)-system
    normalize(_Hist_S_T_Z_cone);

    //Durham distribution
```

```
      normalize(_Hist_Durham);


  }

private:

  double max_eta = 5.; // accelerator max eta
  int nbins = 10; // number of bins

      // Histogram pointers

      // pT
      Histo1DPtr _Hist_pT_T;
      Histo1DPtr _Hist_pT_TBAR;

      // eta
      Histo1DPtr _Hist_eta_T;
      Histo1DPtr _Hist_eta_TBAR;
      Histo1DPtr _Hist_eta_Z;
      Histo1DPtr _Hist_deta;

      // phi
      Histo1DPtr _Hist_phi_T;
      Histo1DPtr _Hist_phi_TBAR;
      Histo1DPtr _Hist_phi_Z;
      Histo1DPtr _Hist_dphi;

      // invariant mass
      Histo1DPtr _Hist_inv_T;
      Histo1DPtr _Hist_inv_TBAR;
      Histo1DPtr _Hist_inv_Z;

      // DeltaR distribution for (muon or antimuon) vs Z cone jet
      Histo1DPtr _Hist_dR_T_Z_cone;

      // sqrtS
      Histo1DPtr _Hist_S_T_Z_cone;

      // Heatmap DeltaR vs sqrtS
      Histo2DPtr _Hist_Lego_T_Z_cone;
```

```
        // Durham distribution
        Histo1DPtr _Hist_Durham;

  };

  // The hook for the plugin system
  DECLARE_RIVET_PLUGIN(TTBAR02);

}
```

Listing 5: **Rivet analysis code for** (higher-energy $\mu$ vs associated particle cone jet)

```
// TTBAR02_all_jet.cc
// -*- C++ -*-
#include "Rivet/Analysis.hh"
#include "Rivet/Projections/FinalState.hh"
#include "Rivet/Projections/IdentifiedFinalState.hh"

#include "Rivet/Tools/Cuts.hh"      // for Cuts
#include "Rivet/Math/Units.hh"      // for GeV
#include <cmath>                    // for M_PI
#include "Rivet/Math/MathUtils.hh"  // for sqr
#include <algorithm>                // for std::min

namespace Rivet {

  /// @brief Add a short analysis description here
  class TTBAR02 : public Analysis {
  public:

    /// Constructor
    DEFAULT_RIVET_ANALYSIS_CTOR(TTBAR02);

    /// @name Analysis methods

    /// Book histograms and initialize projections before the run
    void init() {

        // Initialize and register projections
        const FinalState fs;
        declare(fs, "FS");
```

```
declare(IdentifiedFinalState(fs,13),"T");
declare(IdentifiedFinalState(fs,-13),"TBAR");


// Book histograms
// T... muon, _TBAR... antimuon

// pT - Transverse momentum distribution
book(_Hist_pT_T,"pT_T",nbins,0,1000);
book( _Hist_pT_TBAR,"pT_TBAR",nbins,0,1000);

// eta - pseudorapidity
book(_Hist_eta_T,"eta_T",nbins,-max_eta,max_eta);
book( _Hist_eta_TBAR,"eta_TBAR",nbins,-max_eta,max_eta);
// delta eta (muon vs all cone)
// book(_Hist_deta,"deta",nbins,-5,5);
book(_Hist_deta,"deta",nbins,-0.8,0.8);

// phi - azimuthal angle
book(_Hist_phi_T,"phi_T",nbins,-M_PI,M_PI);
book(_Hist_phi_TBAR,"phi_TBAR",nbins,-M_PI,M_PI);
// delta phi (muon vs all cone)
// book(_Hist_dphi,"dphi",nbins,0,M_PI);
book(_Hist_dphi,"dphi",nbins,0,0.8);

// invariant mass
book(_Hist_inv_T,"inv_T",nbins,0,200);
book(_Hist_inv_TBAR,"inv_TBAR",nbins,0,200);

// DeltaR distribution for the higher-energy (muon or antimuon) vs particle cone jet
book(_Hist_dR_all_cone, "dR_all_cone", nbins, 0, 6);

// sqrtS - invariant mass of the combined muon-all_cone-system
book(_Hist_S_all_cone, "S_all_cone", nbins, 0, 500);

// Heatmap DeltaR vs sqrtS
book(_Hist_Lego_all_cone, "lego_all",nbins, 0, 6,nbins, 0, 500);
//Zoom
//book(_Hist_Lego_all_cone, "lego_all",50, 0, 2,100, 0, 400);

// Durham distribution for higher-energy (muon or antimuon) vs particle cone jet
```

```
    book(_Hist_Durham,"Durham",nbins,-12.0,0.0);
}


/// Perform the per-event analysis
void analyze(const Event& event)
{
    const double weight = event.weight();

    const auto& mus  = apply<IdentifiedFinalState>(event, "T").particlesByPt();
    const auto& amus = apply<IdentifiedFinalState>(event, "TBAR").particlesByPt();
    const Particles& parts = apply<FinalState>(event, "FS").particles();

    if (mus.empty() || amus.empty()) return;


    const double R0 = 0.8;    // Cone-radius

    const Particle& TOP    = mus.front();    // muon
    const Particle& TOPBAR = amus.front();   // antimuon


    // Muon
    const double pT_T  = TOP.pT();
    const double eta_T = TOP.eta();
    const double phi_T = TOP.phi();
    const FourMomentum P_T = TOP.mom();

    _Hist_pT_T  -> fill(pT_T,  weight);
    _Hist_eta_T -> fill(eta_T, weight);
    _Hist_phi_T -> fill(phi_T, weight);
    _Hist_inv_T -> fill(P_T.mass(), weight);

    // Antimuon
    const double pT_TBAR  = TOPBAR.pT();
    const double eta_TBAR = TOPBAR.eta();
    const double phi_TBAR = TOPBAR.phi();
    const FourMomentum P_TBAR = TOPBAR.mom();

    _Hist_pT_TBAR  -> fill(pT_TBAR,  weight);
    _Hist_eta_TBAR -> fill(eta_TBAR, weight);
```

```
_Hist_phi_TBAR -> fill(phi_TBAR, weight);
_Hist_inv_TBAR -> fill(P_TBAR.mass(), weight);

// choosing the higher energy muon or antimuon
const bool takeT = (P_T.E() > P_TBAR.E()) || (P_T.E() == P_TBAR.E() && pT_T >= pT_TBAR);
// kinematics of the higher energy particle
const FourMomentum& P_MU = takeT ? P_T : P_TBAR;
const double eta_MU = takeT ? eta_T : eta_TBAR;
const double phi_MU = takeT ? phi_T : phi_TBAR;

FourMomentum P_cone;

// calculate the particle cone jet
for (const Particle& p : parts) { // take all particles
  if (isNeutrino(p)) continue;   // don't include neutrinos
  // exclude the leading muon from the constructed cone jet
  if (std::abs(p.pid()) == 13) {
    const double dphi_mu_p = deltaPhi(phi_MU, p.phi());
    const double dR_mu_p   = sqrt(sqr(eta_MU - p.eta()) + sqr(dphi_mu_p));
    if (dR_mu_p < 1e-6) continue;
  }
const double dphi_mu_p = deltaPhi(phi_MU, p.phi());
const double dR_mu_p = sqrt( sqr(eta_MU - p.eta()) + sqr(dphi_mu_p) );
  if (dR_mu_p < R0) {
      P_cone += p.mom();
  }
}

// Skip if cone empty
if (P_cone.pT() <= 0) return;

// Kinematics of the particle cone
const double eta_cone = P_cone.eta();
const double phi_cone = P_cone.phi();

// DeltaR distribution for (muon or antimuon) vs particle cone jet
const double dphi = deltaPhi(phi_MU, phi_cone);
const double deta = (eta_MU - eta_cone);
const double dR  = sqrt(sqr(deta) + sqr(dphi));
_Hist_dphi -> fill(dphi, weight);
_Hist_deta -> fill(deta, weight);
```

```
    if (std::isfinite(dR)) _Hist_dR_all_cone->fill(dR, weight);

    // sqrtS - invariant mass of the combined muon-all_cone-system
    const double sqrtS = (P_MU + P_cone).mass();
    _Hist_S_all_cone -> fill(sqrtS, weight);

    // Heatmap DeltaR vs sqrtS
    _Hist_Lego_all_cone -> fill(dR,sqrtS,weight);


    // Durham distribution

    // Measure Energies E_i,E_j
    const double E_j = P_cone.E();
    const double E_i = P_MU.E();
    // Angle between higher energy muon/antimuon and particle cone jet
    double cosTheta = cos(P_MU.angle(P_cone));
    cosTheta = std::max(-1.0, std::min(1.0, cosTheta)); // avoid rounding errors
    const double E_s = sqr(E_i + E_j);
    if (E_s > 0 && std::isfinite(E_s)) {
      // Formula for the durham algorithm
      const double y_ij = (2.0*sqr(std::min(E_i, E_j)) / E_s) * (1.0-cosTheta);
      if (y_ij > 0 && std::isfinite(y_ij)) {
       _Hist_Durham-> fill(std::log(y_ij),weight);
      }
    }
}


/// Normalize histograms etc., after the run
void finalize()
{
    // pT - Histograms for T,TBAR
    normalize(_Hist_pT_T);
    normalize(_Hist_pT_TBAR);

    // eta - Histograms for T,TBAR
    normalize(_Hist_eta_T);
    normalize(_Hist_eta_TBAR);
    normalize(_Hist_deta);
```

```
    // phi - Histograms for T,TBAR
    normalize(_Hist_phi_T);
    normalize(_Hist_phi_TBAR);
    normalize(_Hist_dphi);

    // invariant mass - Histograms for T,TBAR
    normalize(_Hist_inv_T);
    normalize(_Hist_inv_TBAR);

    // DeltaR distribution for higher-energy (muon or antimuon) vs particle cone jet
    normalize(_Hist_dR_all_cone);

    // sqrtS - invariant mass of the combined muon-particle-cone system
    normalize(_Hist_S_all_cone);

    // Heatmap DeltaR vs sqrtS
    normalize(_Hist_Lego_all_cone);

    // Durham distribution for the higher-energy (muon or antimuon) vs particle cone jet
    normalize(_Hist_Durham);


  }

private:

  double max_eta = 5.;
  int nbins = 10; // number of bins

    // Histogram pointers

    // pT
    Histo1DPtr _Hist_pT_T;
    Histo1DPtr _Hist_pT_TBAR;

    // eta
    Histo1DPtr _Hist_eta_T;
    Histo1DPtr _Hist_eta_TBAR;
    Histo1DPtr _Hist_deta;

    // phi
```

```
    Histo1DPtr _Hist_phi_T;
    Histo1DPtr _Hist_phi_TBAR;
    Histo1DPtr _Hist_dphi;

    // invariant mass
    Histo1DPtr _Hist_inv_T;
    Histo1DPtr _Hist_inv_TBAR;

    // DeltaR distribution for the higher-energy (muon or antimuon) vs particle cone jet
    Histo1DPtr _Hist_dR_all_cone;

    // sqrtS
    Histo1DPtr _Hist_S_all_cone;

    // Heatmap DeltaR vs sqrtS
    Histo2DPtr _Hist_Lego_all_cone;

    // Durham distribution
    Histo1DPtr _Hist_Durham;

  };

  // The hook for the plugin system
  DECLARE_RIVET_PLUGIN(TTBAR02);

}
```